Flow discharge and sediment transport models for estimating a minimum timescale of hydrological activity and channel and delta formation on Mars

M. G. Kleinhans

Department of Physical Geography, Faculty of Geosciences, Utrecht University, Utrecht, Netherlands

Received 29 June 2005; revised 12 September 2005; accepted 19 September 2005; published 2 December 2005.

[1] This paper summarizes state-of-the-art models for water flow and sediment transport and suggests implications for the sediment grain size distribution, transport process, and delta formation. The flow velocity in Martian outflow channels is commonly calculated from the Manning equation, which is dimensionally incorrect and masks the large uncertainty of the reconstructed flow velocity. More modern friction predictors based on surface grain size distribution are tested on 190 rivers on Earth including moderately catastrophic events. The uncertainty for the flow velocity is a factor of 3–4. The sediment transport is commonly assumed to amount to 40% of the water flux (hyperconcentration), but this is only true for special conditions. A debris-flow origin of the channels is unlikely. Application of modern sediment transport models to typical Martian conditions indicates orders of magnitude smaller sediment fluxes dominated by bed load transport, resulting in much larger timescales for sediment emplacement in crater lake deltas and in the potential northern ocean. This is in part caused by the unexpected grain size distribution of the sediment derived from observations of landers and of delta morphologies. The implied duration of hydrological activity and channel and delta formation is of the order of 10^3–10^6 years, which is still very short on the geological timescale of Mars.

Citation: Kleinhans, M. G. (2005), Flow discharge and sediment transport models for estimating a minimum timescale of hydrological activity and channel and delta formation on Mars, *J. Geophys. Res.*, *110*, E12003, doi:10.1029/2005JE002521.

1. Introduction

[2] Understanding the physics of water and sediment discharge through outflow channels on Mars is crucial to reconstruct the morphogenesis of the surface [e.g., *Baker and Milton*, 1974; *Komar*, 1979; *Carr*, 1996; *Baker*, 2001]. Moreover, the outflow channels potentially provide information on the past climate and the potential ocean of the northern hemisphere [*Parker et al.*, 1993; *Baker et al.*, 1991; *Baker*, 2001; *Murray et al.*, 2005]. This understanding is still limited; e.g., *Ivanov and Head* [2001] and *Kreslavsky and Head* [2002] identify three key questions, the first of which is: What is the total amount of water and sediment load involved in individual outflow events? The general aim of this paper is to summarize and apply recent terrestrial models and insights of fluvial geomorphology and engineering to Mars.

[3] Various authors addressed the problem of flow discharge estimation but few addressed sediment transport computation on Mars. In two benchmark papers, *Komar* [1979, 1980] summarized the laws of hydraulics to calculate the flow, calculated sediment transport on Mars with the equation of *Bagnold* [1966] and compared the large channels on Mars to catastrophic outflow channels on Earth [*Baker and Milton*, 1974] and to turbidity currents [*Komar*, 1979, 1980]. One important conclusion was that the Manning equation for flow is not properly nondimensionalized [*Silberman et al.*, 1963], but unfortunately many later workers used this equation with a constant Manning coefficient rather than the correct Darcy-Weisbach equation (given later). *Wilson et al.* [2004] assessed the errors of discharge reconstruction and summarized modern friction laws replacing the constant Manning coefficient, but their analysis must be updated because an error was made in the derivation of grain size from lander rock distributions (see section 3).

[4] Another important conclusion of *Komar* [1980] was that sand (defined as $0.063 < D < 2$ mm, wherein D = grain size) and finer particles can be transported in certain conditions as wash load because it requires no net expenditure of water flow power. As in some dense turbidity currents on Earth, the sediment concentration by weight could then be as large as 60–70% of the flow or 40% of volume. This "hyperconcentration" is an important number. For example, a minimum timescale of formation of channels and deposits can be estimated by assessing the volumes of eroded or deposited sediment and the probable sediment transport rate in the channels [*Komar*, 1979]. The volume of sediment divided by the sediment transport rate provides an estimate of the timescale [e.g., *Goldspiel and Squyres*, 1991; *Irwin et al.*, 2004], which is a vital piece of the past

0148-0227/05/2005JE002521$09.00

climate puzzle and may help to decide between scenarios ranging between a cold, dry and windy "white" Mars, and a warm, wet and wild "blue" Mars [*Hoffman*, 2000; *Baker*, 2001] and the duration of such eras.

[5] Unfortunately, this 40% number of *Komar* [1980] for special cases has later been used for all cases without considering the necessary conditions (discussed later), leading to conclusions that are potentially wrong. This doubt was also raised by *Carr* [1996, p. 61]. One characteristic of wash load is that it is limited by the amount of upstream supply [e.g., *Walling and Fang*, 2003], which makes comparison between different regions and planets very difficult. For example, in an otherwise very thorough paper *Kreslavsky and Head* [2002] compare the wash load sedimentation rate in impact craters on the northern hemisphere of Mars to the mud sedimentation rate in a gas pipe line explosion crater in the North Sea on Earth [*Thatje et al.*, 1999]. The mud supply in the North sea is limited by material transported northward through the English Channel out of the Celtic sea, mud derived from erosion of the south-east English coast, and mud derived from the Wadden Sea of the Netherlands and Germany. These conditions are not in the least comparable to that in an ancient ocean on Mars. I will address the question of when the conditions for large sediment concentrations potentially are met (section 6).

[6] If the sediment is not transported as wash load, then it moves as rolling and saltating bed load or as suspended load diffused upward into the flow by the turbulence [*Einstein*, 1950; *Komar*, 1979]. The concentrations are then very much smaller and estimates of the timescale should be much larger. Now the question is how to identify from the deposits which transport mechanism took place. In addition, we then need equations to predict the sediment transport rate. *Komar* [1979] used the equation of *Bagnold* [1966], but since *Komar* [1979] the science of sediment transport has progressed much. I will summarize current knowledge and uncertainties of sediment transport (section 5) and some ramifications for the outflow channels and delta morphologies on Mars.

[7] The application of flow and sediment transport predictors assumes equilibrium conditions, which may easily lead to large bias or wrong conclusions for catastrophic outflow channels. A fluvial channel in equilibrium is fully determined by the boundary conditions discharge, water level and slope, and equations for mass conservation of water and sediment, a friction law, a sediment transport law and a predictor or specification for channel width. If one variable is unknown it can be calculated from the other variables. For example, *Jerolmack et al.* [2004] used an existing set of equations for alluvial fans to solve for discharge to the Holden NE fan. This is not without risk, however. *Thiebodeaux et al.* [2003] employ another possible set of equations to solve for grain size, but friction and sediment transport laws have large uncertainties on Earth (see section 2). Moreover, the sediment transport rate depends nonlinearly on flow velocity. Also, the width of a channel is very uncertain and highly dependent on the stage and the intricacies of poorly constrained bank erosion processes and the narrowing process of the channel by deposition. These uncertainties add up to an uncertainty of orders of magnitude for the grain size. As a result, a grain size may be predicted that is not even present in the source material. In other words, a large range of grain sizes may be obtained depending on the choice of roughness and sediment transport equations.

[8] In short, there is a need for a defendable set of equations for flow and sediment discharge applicable on Mars, which is the aim of this paper. First I summarize the hydraulic laws for water flow and compare characteristic nondimensional numbers for rivers on Earth (section 2). Next, the available information on the sediment grain size distribution in Martian channels is interpreted (section 3). Then the sediment mobility is calculated and a rational framework for the prediction of subaqueous bed forms is given (section 4). This is relevant for the friction and the transport dynamics. Then, some sediment transport laws are given and their results for Martian conditions calculated (section 5). On the basis of this, two alternative necessary conditions for wash load and hyperconcentrated flows are reviewed (section 6). The discussion will focus on the limitations and consequences of the updated sediment transport theory for the formation time of channels (section 7.1) and delta deposits (section 7.2) on Mars, as well as constraints for the grain size distribution of the sediment and groundwater aquifer reloading (section 7.5). Finally, as an example, flow and sediment transport predictions are compared between various channels on Mars on the basis of earlier and the present work.

2. Flow Computations

2.1. Flow Velocity and Discharge

[9] The flow discharge is relevant for climatic studies and the fate of crater lakes and the ocean. The flow discharge (=volume flux in m^3/s) is given as

$$Q = hWu \tag{1}$$

where h = water depth, W = channel width and u = flow velocity averaged over the depth and width of the channel. The channel width can be derived from images. The velocity has to be estimated using a friction law and a measured depth from altimetry data. Over- or underestimating the depth not only affects the discharge but also indirectly the velocity through the roughness equation (shown below). This effect is ignored in the Manning equation which masks this additional uncertainty. For Martian channels, the depth is sometimes difficult to constrain. The maximum depth obviously is slightly larger than bankfull, while the minimum depth may be indicated by terraces. The terraces and channel floor morphology may also indicate modification of the channel depth by secondary processes such as glacial and periglacial processes.

[10] The equations for flow and sediment transport are commonly applied to bankfull discharge because on Earth it is reasonable to assume that this is the channel forming discharge for fluvial channels [*Leopold et al.*, 1964]. Smaller floods on Earth have less energy and are thus unable to do much work, even though these occur most frequently. Larger floods potentially do a lot of work but are rare and therefore also are assumed to have a limited effect [*Wolman and Miller*, 1960]. In reality, most rivers on Earth are to some extent in disequilibrium and are continuously

adapting to changing boundary conditions (climate, base level and tectonics) and extreme events. It is not known how well the bankfull discharge paradigm is applicable to channels generated by catastrophic events only. Moreover, it is not known whether the Martian channels are truly fluvial (formed in their own deposits) or are, like bedrock rivers on Earth, detachment limited in transport because the sediment has to be scoured from the hardrock bed and banks (see section 7).

[11] Both the channel floor and walls cause friction for the flow. Assuming the floor and wall roughness to be equal (which is reasonable), the effect of walls on the water depth is incorporated in the hydraulic radius of cross-sectional area divided by wetted perimeter:

$$R_h = \frac{Wh}{W + 2h} \tag{2}$$

which approaches h for wide channels. Hereafter the hydraulic radius is called water depth for simplicity.

[12] The depth- and width-averaged flow velocity is calculated from the Darcy-Weisbach equation (in *Silberman et al.* [1963]):

$$u = \sqrt{\frac{8ghS}{f}} \tag{3}$$

where g = acceleration due to gravity (9.81 m/s^2 on Earth and 3.74 m/s^2 on Mars), h = depth (hydraulic radius) and S = energy slope of the flow, for steady and uniform flow equal to the water surface slope and channel bed surface slope (in m/m, not in degrees). The similar Chezy equation is

$$u = C\sqrt{hS} \tag{4}$$

and the Manning equation is

$$u = \frac{h^{2/3}S^{1/2}}{n} \tag{5}$$

As a result of the above, the friction factor f is related to the Chezy (C) and Manning (n) roughness coefficients as

$$C = \sqrt{\frac{8g}{f}} \tag{6}$$

$$n = h^{1/6}\sqrt{\frac{f}{8g}} \tag{7}$$

2.2. Friction Factors

[13] Now the problem is to find a predictor for f. The hydraulic roughness problem is notorious in civil engineering. The roughness is a highly relevant parameter because it determines water depth and therefore artificial levee design. However, the roughness is a complicated outcome of the interactions between flow, flow turbulence, the added resistance of transported sediment, and most importantly roughness elements such as grains on the bed and bed forms. In practice it is therefore commonly used as calibration parameter in flow models, or derived from measurements of the other parameters in equation (3) which explains the large number of available predictors. Consequently, the predictors have applicability ranges determined by the data set they were derived from.

[14] A general and well-verified roughness predictor is the White-Colebrook function [*Silberman et al.*, 1963]:

$$\sqrt{\frac{8}{f}} = 5.74\log_{10}\left(12.2\frac{h}{k_s}\right) = 5.74\log_{10}\left(\frac{h}{k_s}\right) + 6.24 \tag{8}$$

in which k_s = Nikuradse roughness length (in m) commonly related to some grain size percentile of the mass frequency distribution, e.g., the D_{50}, D_{84} or D_{90} (see section 3) or to bed form height (see section 4). *Wilson et al.* [2004] review a number of predictors. The most relevant are their equations (14) and (7b):

$$\sqrt{\frac{8}{f}} = 5.75\log_{10}\left(\frac{h}{D_{84}}\right) + 3.514 \tag{9}$$

$$\sqrt{\frac{8}{f}} = 7.515\left(\frac{h}{D_{50}}\right)^{0.1005} S^{-0.03953}\sigma_g^{-0.1283} \tag{10}$$

in which the friction also depends on channel slope S and the geometric standard deviation σ_g of the sediment grain size distribution, approximated for logarithmic distributions as

$$\sigma_g = \frac{1}{2}\left(\frac{D_{84}}{D_{50}} + \frac{D_{50}}{D_{16}}\right) \tag{11}$$

[15] The friction laws assume hydraulic rough conditions, which is the case when grains protrude into the flow above the laminar sublayer $\delta \approx 11.63\ \nu/u^*$, or, expressed as a Reynolds shear velocity number,

$$Re^* = \frac{u^* D_{50}}{\nu} \tag{12}$$

where $Re^* < 3.5$ indicates laminar flow, $Re^* > 70$ indicates turbulent flow and $Re^* = 11.63$ is defined as the transition. The conditions are always rough for Martian channels. The ν = kinematic viscosity of water is only slightly dependent on water temperature water as $\nu \approx 4 \times 10^{-5}/(20 + t)$ where t = temperature in °C. Here $\nu = 1.6 \times 10^{-6}$ is used for 3°C.

2.3. Test of Friction Factors on Rivers on Earth

[16] Herein, these predictors and other flow and sediment mobility parameters are compared with a large data set of rivers on Earth. This data set contains 190 rivers of different planforms, namely straight, meandering and braided with both sand and gravel bed sediment, and including 10 catastrophic channels created in glacial

outburst events over 10 braided gravel channels in Nepal. The size of the rivers varies between small streams and the Mississippi river at St. Louis and other large rivers from most continents. The straight, meandering and braided rivers are from *Parker* [2005] and *Van den Berg* [1995] and the catastrophic channels are from *Cenderelli and Wohl* [2003]. All parameters in the data set refer to bankfull flow conditions except those of the catastrophic channels.

[17] In addition, a new roughness predictor is calibrated on the full data set to illustrate the variation introduced by taking just another data set (even though this is a very extensive one containing many gravel rivers and some catastrophic channels). The result is

$$\sqrt{\frac{8}{f}} = 2.2\left(\frac{h}{D_{50}}\right)^{-0.055} S^{-0.275} \tag{13}$$

The roughness predictors are compared with the data in Figures 1 and 2. Not surprisingly the new equation fits the best to the data it was derived from.

[18] Four important observations come out of this analysis, partly in agreement with *Wilson et al.* [2004]. First, empirical roughness clearly depends on both the relative roughness ratio h/D_{50} and channel slope S (Figure 1). Second, the variation between roughness predictors is considerable; the trends may be very different (Figure 1) which will greatly affect predicted flow velocities on Mars. A retrodiction based on various roughness predictors (Figure 2) clearly shows that the true flow velocity is overestimated with more than a factor of three using the equations listed by *Wilson et al.* [2004]. Using a constant Manning coefficient of $n = 0.0545$ results in large errors. Third, the scatter is large, especially for the sand bed channels which is due to bed form roughness. The relatively larger roughness in sand bed rivers is further confirmed in Figure 3, where the empirical Nikuradse roughness length derived from the data using equation (8) is much larger than the grain roughness. It remains to be seen, however, how relevant the sand bed river and bed form phenomena are for the Martian channels (see sections 3 and 4). Fourth, it is fortunate that the validity range of the relative roughness and the slope envelop those of the Martian channels. This can be calculated from the parameters given in this paper. It is obvious, however, that the uncertainty related to flow velocity and discharge reconstruction of Martian channels is large, say, a factor of three.

[19] For debris flows, a similar approach can be used to predict the flow velocity. Various friction predictors were tested by *Rickenmann* [1999], who found that a single equation could be used for water and debris flows with comparable uncertainties as found in this paper.

2.4. Reynolds and Froude Numbers

[20] Two other parameters are needed to describe the nature of the flow. The Reynolds number of the flow Re_f indicates whether the flow is turbulent (for $Re_f > 500$):

$$Re_f = \frac{uh}{\nu} \tag{14}$$

The flow is always turbulent for rivers on Earth and channels on Mars (Figure 4) which makes this number redundant.

[21] The Froude number defines the transition between subcritical and supercritical flow at $Fr = 1$ (or $Fr = 0.84$ for bed forms [*Southard and Boguchwal*, 1990]). Moreover, equation (10) is only valid for critical and supercritical flow. The Froude number is given as the ratio of flow velocity and shallow flow wave celerity:

$$Fr = \frac{u_c}{\sqrt{gh}} \tag{15}$$

As such, it indicates whether the flow is affected by downstream (subcritical, $F < 1$) or upstream (supercritical, $F > 1$) effects such as constrictions, changes in hydraulic roughness or ponding in a lake or ocean. Interestingly, many sand bed rivers have $F < 1$ while many gravel bed rivers have $F < 1$ and $F \approx 1$ (Figure 4). This number therefore has great significance for channel flow.

2.5. Total and Grain-Related Bed Shear Stress

[22] The bed shear stress is necessary for the computation of sediment transport which, together with the delta volume, determines delta formation timescale (see section 7.1). It can be derived from the force of a block of water of unit length and width and with water depth h on the channel bed which is at slope S. The bed shear stress (in N/m^2 or Pa) becomes

$$\tau_c = \rho u^{*2} = \rho g h \sin S \tag{16}$$

It is obvious now that any uncertainty in water depth directly translates in an uncertainty in shear stress. The slope is commonly rather well constrained by altimetry measurements in the dry channels of Mars. In addition, the computation of shear stress and hence of sediment transport hinges on the assumption of bankfull discharge. Combination with the Darcy-Weisbach friction (equation (3)) [*Silberman et al.*, 1963], shear stress is given by

$$\tau_c = \frac{1}{8}\rho f_c u_c^2 \tag{17}$$

[23] The total shear of the flow is related to the total friction of the channel. For the computation of near-bed sediment transport, however, only the shear force on the grains is needed. *Einstein* [1950], *Soulsby* [1997], and others conceptually divided the total shear stress into bed form-related shear stress and grain-related shear stress, of which the latter is relevant for sediment transport. The grain shear stress is calculated from equation (17) with the White-Colebrook friction law (equation (8)), where the hydraulic roughness length is chosen as $k_s = D$.

[24] An important choice to make is the D. Many options have been discussed in the literature [see, e.g., *Van Rijn*, 1984a, and references therein] but the most common are $k_s = 2.5D_{50}$ or $k_s = D_{90}$. For many sediments these are almost the same. In this paper $2.5D_{50}$ for the data set of rivers on Earth (for which D_{90} is not

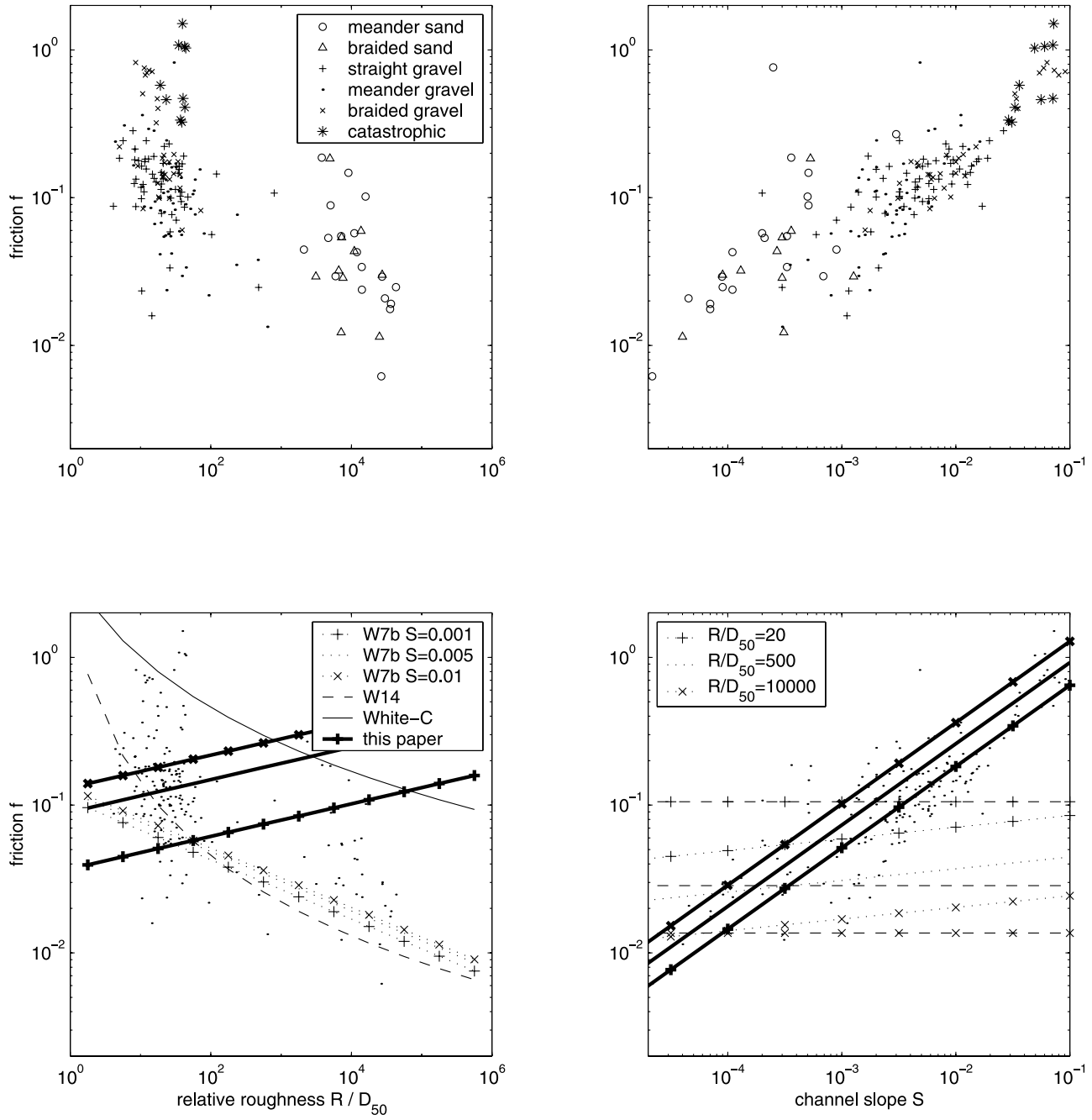

Figure 1. Darcy-Weisbach friction factors for various channels on Earth (bankfull flow) and a test of friction predictors based on R/D_{50} and slope S. "W7b" and "W14" refer to equations (7b) or (14) of *Wilson et al.* [2004] (equations (10) and (9) herein). "White-C" refers to equation (8) with $k_s = 2.5D_{50}$. The roughness predictor "this paper" refers to equation (13) and was calculated for the same three S or R/D_{50} as the "W7b".

given) and D_{90} is used for Martian channels because the D_{90} can be determined more accurately from rock counts than the D_{50} as explained in the next section.

3. Grain Size Distribution of the Sediment

[25] The grain size distribution of the transported and deposited sediment is an important input parameter for the roughness and for the sediment transport predictors, in specific the D_{50} and D_{90} percentiles of the mass frequency distribution. The most important source of information is from lander images. Rock size frequencies by number (not mass) demonstrate dominance of gravel and cobble sized sediments mostly between 0.01–1 m [*Golombek et al.*, 2003] but, notably, also sand of 0.1–2 mm [*Fenton et al.*, 2003; *Grotzinger and Athena Science Team*, 2004; *Herkenhoff et al.*, 2004], and the presence of atmospheric dust of a few μm (which will further be ignored).

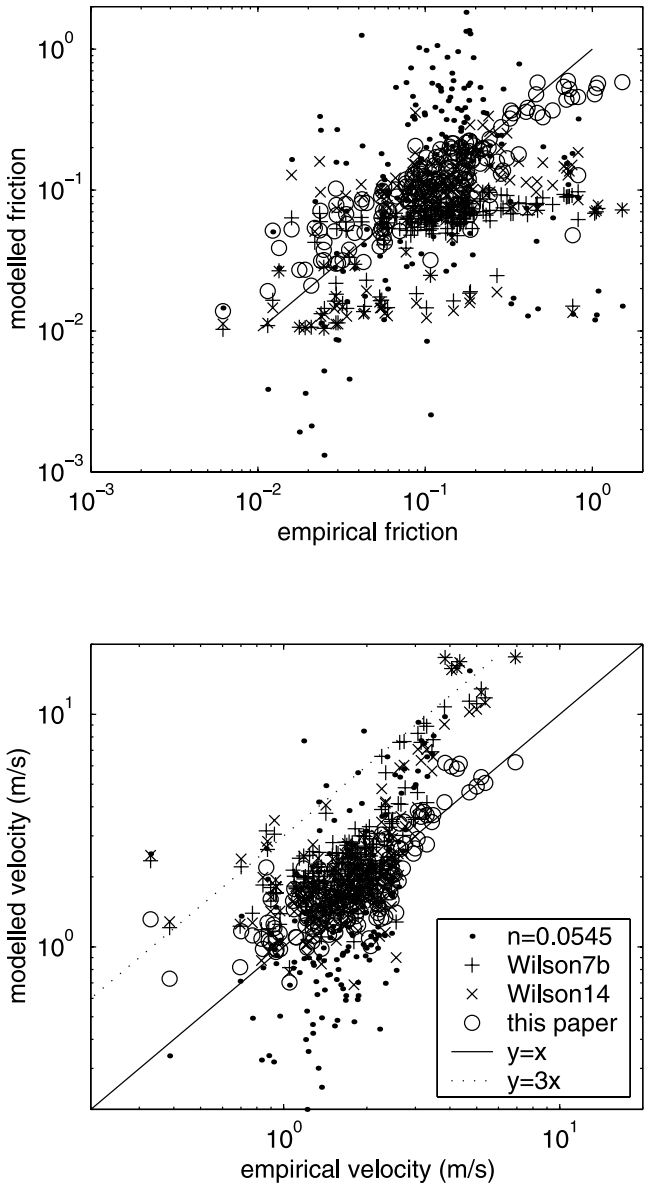

Figure 2. Performance of friction predictors and predicted flow velocity tested on channels on Earth.

[26] *Wilson et al.* [2004] summarized the rock data in percentiles (their Table 1; see Table 1) to use as roughness lengths in the hydraulic roughness equations. There are four problems with their method and with the data. First, these landers obviously sampled in the relatively smooth plains downstream of outflow channels mostly for landing safety so the grain size distributions may be a poor sample of the uplands. It is also conceivable that the rocks have a volcanic origin and were not emplaced by the flows. Second, surface sampling systematically underrepresents the finer sediment. There is obviously a resolution limit for the camera, but the large cobbles also shield the smaller grains from sight. However, it is the best available at the moment.

[27] Third, the frequency distributions of *Golombek et al.* [2003] and *Herkenhoff et al.* [2004] are by number of grains rather than mass as is necessary for the (calibrated) roughness and sediment transport predictors [e.g., *Krumbein and Pettijohn*, 1938]. Conversion is necessary as

$$p_{i,m} = \frac{p_{i,n} \times \frac{4}{3}\pi\left(\frac{D_i}{2}\right)^3}{\sum_i \left[p_{i,n} \times \frac{4}{3}\pi\left(\frac{D_i}{2}\right)^3\right]} \tag{18}$$

where $p_{i,m}$ = mass probability of fraction i, $p_{i,n}$ = probability by number of stones and D_i = diameter of grain size fraction, logaritmically interpolated between the class boundaries. The cumulative probability is calculated by summing the fractional probabilities. The maximum cumulative probability is unity for the upper class boundary of the largest observed grain size bin. The results are given in Figure 5. Unfortunately, the grain sizes are now four times larger than assumed by *Wilson et al.* [2004], which has consequences for the flow velocity (discussed later).

[28] Fourth, a mixture of grains commonly develops a coarse layer at the surface, known in fluvial literature as armor layer and in aeolian literature as desert pavement. Finer material is removed by water or air flow and deposited elsewhere. Moreover, the slightest movement of grains dilates the mixture and allows fines to percolate downward through the pores of the larger particles, known as kinematic sieving. Consequently, surface sampling under-samples the fines which are present in larger proportions in the underlying sediment. There are corrections for the kinematic

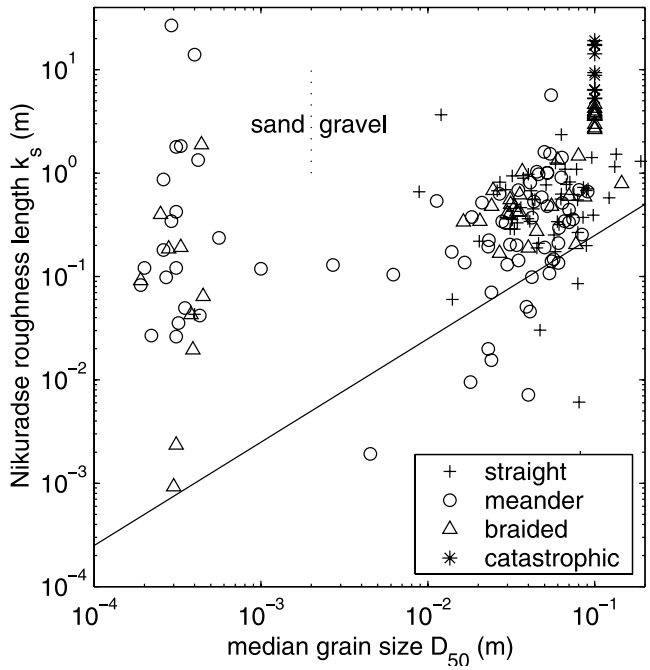

Figure 3. Nikuradse roughness length derived from the friction factors. The line $y = x$ indicates where the roughness is equal to an estimate of grain roughness D_{50}. The sand-bed channels generally have larger roughness lengths due to presence of bed forms.

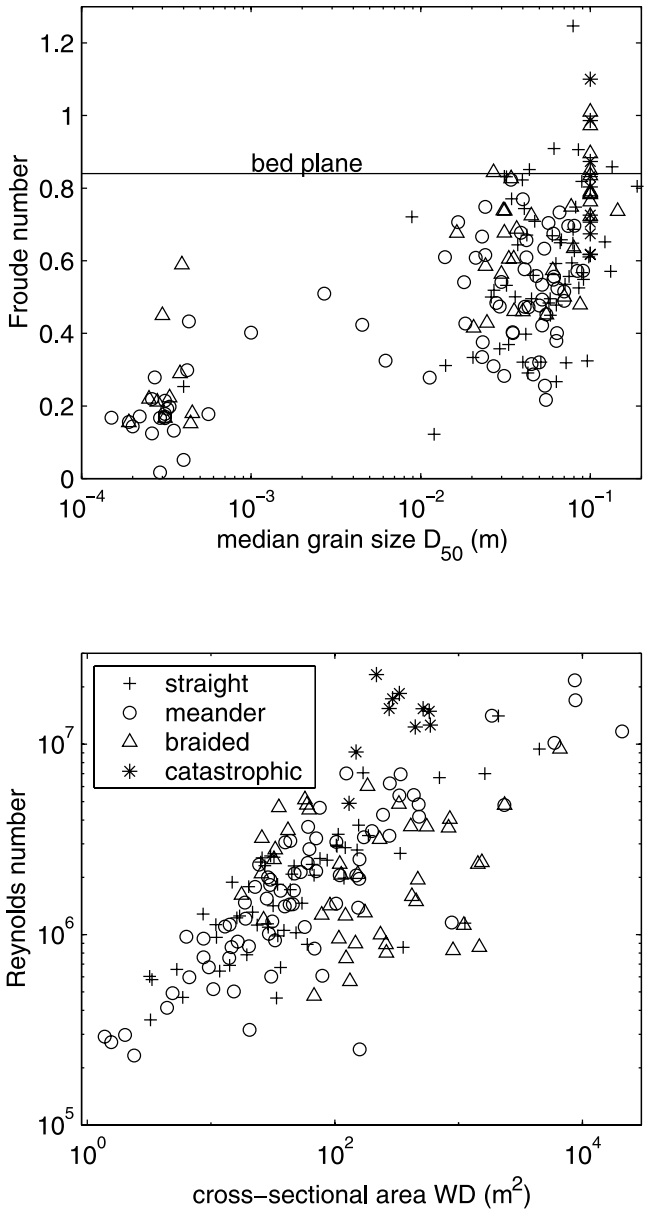

Figure 4. Froude and Reynolds numbers of the channels on Earth. The bed is plane for $Fr > 0.84$ and may develop antidunes for larger Froude numbers. The flow is turbulent for $Re \gg 500$, which is nearly always the case in channels on Earth and Mars.

Table 1. Grain Size Percentiles (in m) of the Fluvial Sediment

D_{10}	D_{50}	D_{90}	Remarks
0.014	0.064	0.209	from frequency of numbers[a]
0.071	0.24	0.63	Pathfinder, corrected (see text)
0.0001	0.0004	0.0008	sand rough estimates[b]
0.0012	0.0014	0.0017	sand[c]
0.0003	0.1	0.6	assumed in this paper

[a] *Wilson et al.* [2004], their average.
[b] *Grotzinger and Athena Science Team* [2004].
[c] *Herkenhoff et al.* [2004].

sieving effect [*Diplas and Fripp*, 1992; *Marion and Fraccarollo*, 1998], of which the most appropriate is

$$p_{i,c} = \frac{p_{i,m} D_i^x}{\sum_i \left[p_{i,m} D_i^x \right]} \tag{19}$$

wherein $p_{i,c}$ = corrected mass probability of fraction $i$and x = exponent which is -0.42 for void-dependent methods such as sampling by wax and -1 for void-independent methods such as photographic sampling (as in this case). Calibration shows that in general $-0.42 < x < -1$. As a result, the finer sediment is now slightly better represented (Figure 5 and Table 1).

[29] Nevertheless, the Martian surface has been subjected to severe wind ablation over billions of years since the sediments were deposited by outflow events, giving ample opportunity for further modification of the surface layer. Rock size distributions from lander photographs are therefore probably not representative for the fluvial sediment. This is also indicated by the finding of sand of 0.1–0.8 mm [*Fenton et al.*, 2003; *Grotzinger and Athena Science Team*, 2004; *Herkenhoff et al.*, 2004]. For further computations an assumption is necessary for the D_{50} and D_{90} of the sediment (and a sensitivity analysis for grain size). There are two ends of the spectrum of possibilities (Figure 5): a unimodal size distribution ranging from fine sand to 1 m cobbles, or a bimodal size distribution with the same range but the fine gravel missing as indicated by the lander findings. Bimodal sediment is common in fluvial environments due to the intricacies of the weathering and transport processes [*Powell*, 1998]. For further computations modified grain size percentiles from a bimodal distribution with 30% of fines are assumed (Table 1). In section 7.5 another argument

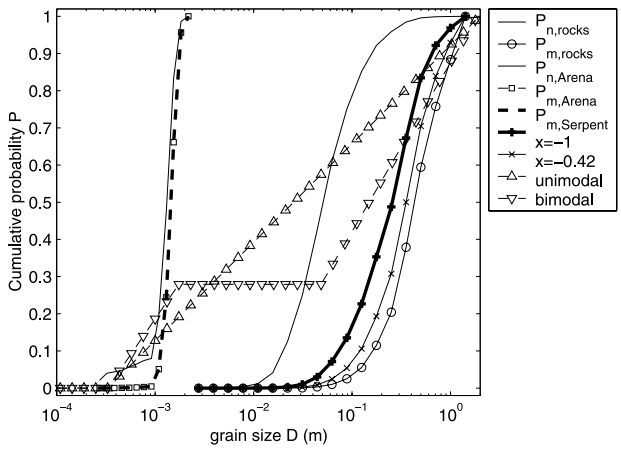

Figure 5. Grain size distributions by number derived from Pathfinder data [*Golombek et al.*, 2003] for rocks and Spirit data [*Herkenhoff et al.*, 2004] for sand, recalculated to distribution by weight. The rock distribution was corrected for surface sampling (power $x = -1$ is preferred; see text). The sand grain size distributions of the Peak Arena wind ripples and of the Serpent sand dune are indistinguishable on this scale. The large skewness to large grain sizes indicates depletion of finer sediments. Two hypothetical distributions of the original sediment are shown (bimodal is preferred).

will be given for bimodal sediment. The assumed grain sizes are clearly very uncertain.

4. Sediment Mobility and Bed Forms

4.1. Earlier Work

[30] Bed forms such as current ripples and dunes are created in certain flow conditions. As a feedback, the bed forms cause a larger hydraulic roughness for the flow. It is therefore essential to understand their conditions of formation. In addition, finding fossil bed forms or associated sedimentary stratification provides an indication for the flow conditions during their generation. This has just become possible on Mars [*Grotzinger and Athena Science Team*, 2004; *Burr et al.*, 2004] but is much more common in terrestrial sedimentology and geology.

[31] In the past, empirical phase diagrams were developed that show the regimes in which various bed states, e.g., bed forms and upper stage plane bed or sheet flow, are stable [e.g., *Simons et al.*, 1965; *Southard and Boguchwal*, 1990]. There are various problems with these older diagrams. *Simons et al.* [1965] presented a diagram with grain size and flow velocity based on flume experiments (also used by *Grotzinger and Athena Science Team* [2004]). Its fatal flaw is that bed states in critical and supercritical flow are included, which depend on the Froude number. The criterion for supercritical flow may occur at any mobility, also below initial motion and above upper stage plane bed depending on the water depth and flow velocity. Moreover, it is not valid for Martian gravity because the flow velocity is not nondimensionalized. *Southard and Boguchwal* [1990] presented an authoritative set of empirical diagrams with nondimensional variables of flow velocity and grain size, accounting for temperature (viscosity) and gravity effects. The diagrams were drawn for various water depths and have fields for lower stage plane bed (plane bed with no sediment movement), current ripples (equilibrium dimensions independent of flow conditions with 0.02–0.05 m height and 0.2–0.5 m length), two- and three-dimensional dunes (dimensions depending on flow conditions), various transitional fields and upper stage plane bed (high energy conditions where bed forms are planed off and the upper few grains of bed sediment are in motion as sheet flow). *Van den Berg and Van Gelder* [1993] collapsed these diagrams into one diagram by removing the water depth effect which is caused by bed form drag. They introduced nondimensional grain shear stress (Shields parameter) rather than flow velocity or total shear stress, following the grain shear stress concept of *Van Rijn* [1984a]. *Kleinhans* [2005b] developed diagrams for currents and waves with rational rather than empirical functions for the lines separating the bed states, which is probably more applicable to another planet.

4.2. Parameters

[32] At least eight variables are found to be needed to characterize bed states in cohesionless sediment of uniform density, sub-spherical shape, approximately logarithmically distributed sediment grain sizes, constant hydrodynamic conditions and large water depth (relative to grain size) [*Southard*, 1971; *Southard and Boguchwal*, 1990]. It is attractive to use nondimensional variables for reducing the number of axes and for larger applicability of the diagrams. Two nondimensional groups suffice, as most natural variation is captured in the flow parameters and sediment sizes. Two variables are needed for the flow: water depth h and the velocity of the currents u_c. The liquid is characterized by its density ρ and viscosity ν. The sediment is characterized by grain diameter D and density ρ_s.

[33] The grain size is here given as the Bonnefille number (in *Van Rijn* [1984a]):

$$D^* = D_{50}\sqrt[3]{\frac{Rg}{\nu^2}} \tag{20}$$

wherein $R = (\rho_s - \rho)/\rho$ is relative submerged density, ρ = fresh or sea water density (1000–1025 kg m^{-3}), ρ_s = sediment density (2650 kg m^{-3} for quartz, 3400 kg m^{-3} assumed for Martian basaltic rock), D_{50} = 50% or median grain size. Alternatively, the particle Reynolds number is often used:

$$Re_p = D_{50}^{3/2}\frac{\sqrt{Rg}}{\nu} \tag{21}$$

[34] Three types of flow parameters are commonly used: based on current velocity, shear stress (τ, including bed form friction) and grain shear stress (τ', only skin friction). Following *Van Rijn* [1984a], the grain shear stress is estimated by equating the k_s in equation (8) to a representative grain size, e.g., $k_{sc} = 2.5D_{50}$, D_{90}, or $3D_{90}$. The shear stress is nondimensionalized as a "Shields parameter":

$$\theta = \frac{\tau}{(\rho_s - \rho)gD_{50}} \tag{22}$$

The Shields parameter for skin friction (θ') is the best defendable choice [*Van den Berg and Van Gelder*, 1993] and is empirically equivalent to other options [*Kleinhans*, 2005b].

4.3. Predictive Bed State Criteria and Diagram

[35] Three physically based functions define four bed state stability fields (Figure 6): incipient motion, ripples, dunes and upper stage plane bed. Note that the functions represent somewhat gradual transitions rather than very hard criteria. Incipient motion is given by the Shields curve for which various curve-fits have been provided [e.g., *Soulsby*, 1997]. Here it is calculated with the physical *Zanke* [2003] model, which collapses on one curve for Earth and Mars (Figure 6) and which can be approximated for practical purposes for $0.05 < D < 5$ mm as

$$\theta_{cr} = \left(0.145Re_p^{-0.333} + 0.045 \times 10^{-1100Re_p^{-1.5}}\right) \tag{23}$$

For $D > 5$ mm the θ_{cr} is that for $D = 5$ mm (Figure 6).

[36] The transition between current ripples and dunes coincides more or less with the transition between hydraulic rough and smooth flow at $Re^* = 11.63$ (equation (12)) [*Allen and Leeder*, 1980; *Kleinhans*, 2005b].

[37] The transition to (subcritical) sheet flow (upper regime plane bed) conditions in currents was theoretically predicted by *Bagnold* [1951] to coincide with a large near-

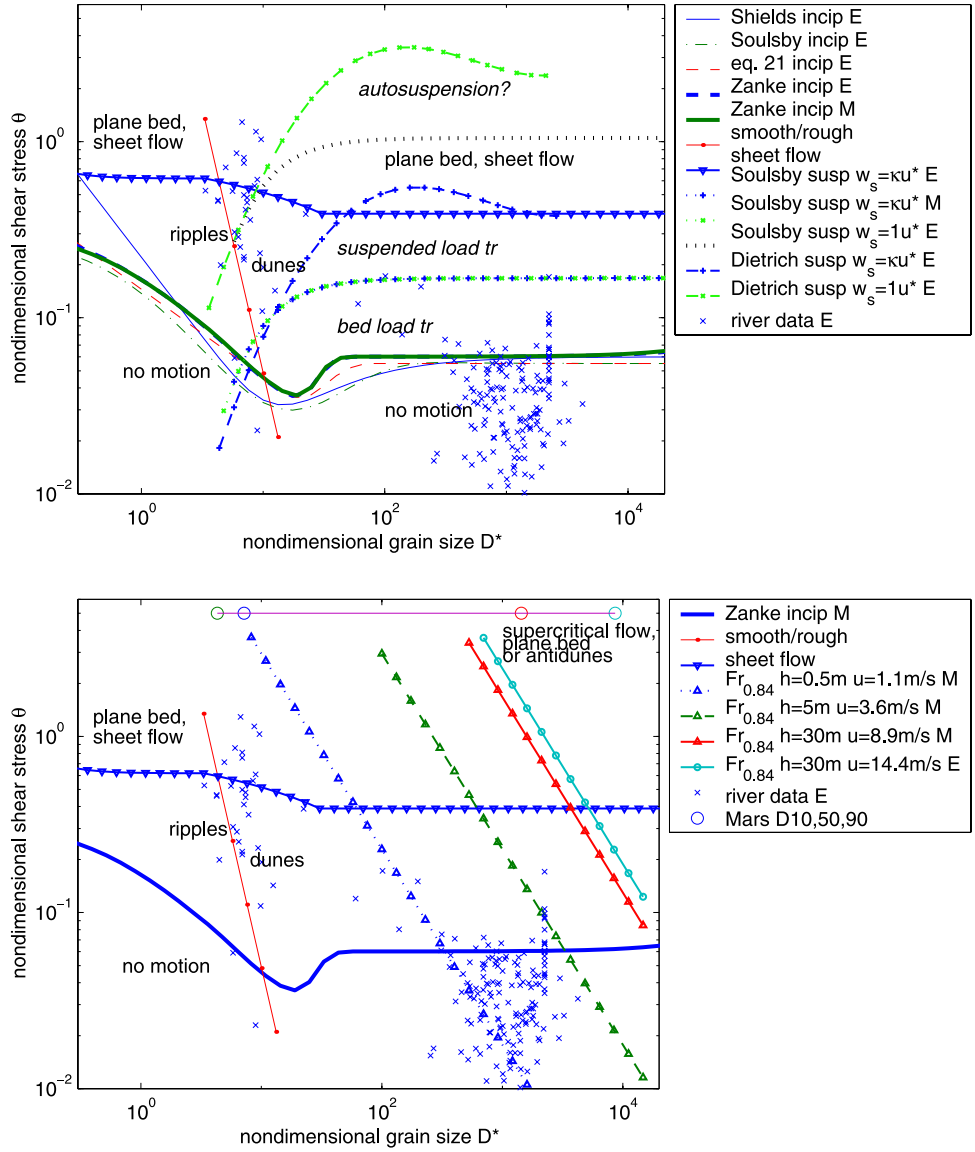

Figure 6. Bed states and sediment mobility (divided over two plots for clarity). Except for the Froude number all curves collapse on top of each other for Earth and Mars. Various criteria for incipient motion are given to demonstrate the limited variability (fit through the original Shields data and *Soulsby* [1997] and *Zanke* [2003]). The transition between hydraulic smooth and rough indicates the transition between ripples and dunes. The sheet flow criterion indicates when the bed forms are planed. Froude numbers larger than 0.84 indicate supercritical flow. Note the large differences between suspension/wash load criteria of *Dietrich* [1982] and *Soulsby* [1997]. The river data are the same as in Figure 1.

bed sediment concentration which damps the turbulence. This was confirmed in experiments. *Allen and Leeder* [1980] modified the *Bagnold* [1951] criterion for UPB for both ripple and dune conditions. The *Allen and Leeder* [1980] criterion is given by

$$\theta_{cr} = c_0 \tan\varphi \tag{24}$$

in which c_0 = maximum bed surface sediment concentration ($c_0 = 1 - \lambda$, where λ is the porosity), φ = angle of repose in radians ($\varphi = 0.95 \approx 43^\circ$ for $D < 0.2$ mm and $\varphi = 0.52 \approx 27^\circ$ for $D > 2$ mm) with intermediate values in between. *Allen* [1984] reviews the c_0 for various grain sizes and mixtures: the $c_0 = 0.65$ for $D < 0.0002$ m and $c_0 = 0.75$ for $D > 0.002$ m with intermediate values in between.

[38] In addition, criteria for supercritical flow and for suspension are given. Critical flow and the associated plane bed (and antidunes in supercritical flow) is shown (Figure 6) for a few combinations of water depth and flow velocity giving $Fr = 0.84$. The critical flow plane bed simply truncates the diagram at various levels. As a result, many gravel-bed streams which would develop dunes for a given shear stress will have a plane bed due to the large Froude number.

[39] An additional sediment mobility criterion for suspension is used later in the sediment transport computations. Suspension is reached when the settling velocity of sedi-

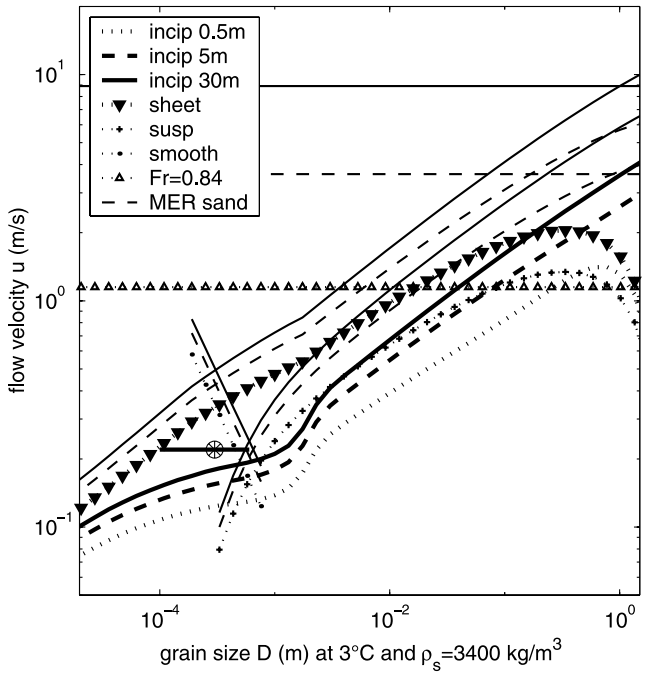

Figure 7. Bed states and sediment mobility in dimensional space for Martian conditions. Figure 6 was converted for three water depths (0.5, 5, and 30 m) with equation (17) and equations (13) and (8) for total and grain roughness ($2.5D_{50}$). Note the large effect of water depth on the truncation of the diagram by supercritical flow. The bed form and sediment mobility fields are the same as in Figure 6. The * indicates the bed form stability field for the ripple stratification in 0.1–0.6 mm sand observed at the MER Opportunity landing site [*Grotzinger and Athena Science Team*, 2004], indicating the possible flow velocity and water depth combinations. The gravel of Mars is in the far right-hand side of the diagram. Note the erratic curves for 0.5 m depth due to exceeding the validity range of the roughness predictor.

ment approaches the shear velocity of the flow. The shear velocity represents turbulent fluctuations in the flow that carry the suspended sediment. The onset of suspension is gradual, but is here chosen at $w_s = \kappa u^*$ [*Van Rijn*, 1984a] where $\kappa = 0.4$ is the von Kármán constant, and the onset of wash load or ''full suspension'' occurs at $w_s = u^*$ [*Bagnold*, 1966]. The settling velocity has been described in many empirical fits with different results. To indicate the observed range, two predictors are given here. The *Soulsby* [1997] predictor is given as

$$w_s = \frac{\nu}{D}\left(\sqrt{10.36^2 + 1.049D^{*3}} - 10.36\right) \tag{25}$$

The nondimensional predictor of *Dietrich* [1982] is

$$\frac{w_s}{\sqrt{RgD}} = \sqrt[3]{\frac{10^Y}{Re_p}} \tag{26}$$

$$Y = \sum_{i=0}^{4} \chi_i \log_{10}\left(Re_p^2\right)^i \tag{27}$$

wherein $\chi_0 = -3.76715$, $\chi_1 = +1.92944$, $\chi_2 = -0.09815$, $\chi_3 = -0.00575$ and $\chi_4 = +0.00056$. Note that this polynomial function cannot be used for $D^* > 1000$.

[40] The same river data as used in the roughness analysis is plotted for comparison (Figure 6). The grain roughness (equation (8)) was used to calculate the nondimensional shear stress, which is valid because at incipient motion and sheet flow the bed is essentially plane so the roughness is grain-related only [*Van den Berg and Van Gelder*, 1993]. The sand-bed rivers on Earth cluster in the dune and ripple fields and above the criterion for suspension and sheet flow. Large sand-bed rivers on Earth near the sheet flow criterion commonly have duned beds which is explained by the tardy reaction of the large dunes to fast-changing flow. Gravel-bed rivers on the other hand cluster only in the bed load and dune fields and in the no-motion field, which reflects the low sediment mobility common for these rivers. The mobility in Martian channels is higher as will be shown later, but note that present-day smooth channel floors on Mars may be the result of dust infilling rather than plane fluvial beds.

[41] Finally, the diagram is recalculated to dimensional space for Martian conditions in Figure 7. Plotting in dimensional space means that the curves are not valid for another planet and sediment density. Again the grain-related roughness function (equation (8)) was used for this. The dimensional diagram (Figure 7) allows direct evaluation of the combination range of flow velocities and water depths for the current ripple stratification and dune morphology found by *Grotzinger and Athena Science Team* [2004] and *Burr et al.* [2004].

5. Sediment Transport

5.1. Sediment Transport Problem

[42] There is an illustrative legend of a conversation between Albert Einstein and his son Hans Albert Einstein, wherein the son starts studying sediment transport, upon which the father remarks that he prefers the more simple problem of general relativity because it has fewer variables. It is important to note that the sediment transport problem is as notorious as the roughness problem: although proper dimensional analysis is applied, a calibration of the constants is necessary and the differences between various predictors are considerable. Moreover, the validity range of flow velocity, depth and grain size associated to the calibration are limited and Martian conditions are well beyond these ranges. Finally, measuring sediment transport is an art in itself with the struggle against the large natural variability, disturbance of the process by measurement instruments and hence scatter and bias in the calibrated predictors. Consequently, hundreds of predictors exist, of which only a few common ones will be presented below. Fortunately, the aim in this paper is not to predict morphological change for a societally relevant engineering problem, but only to assess the order of magnitude of sediment transport on Mars, which is possible despite the scatter.

[43] Sediment transport is conceptually divided into rolling and saltating bed load, and suspended load diffused upward into the flow by the turbulence [*Einstein*, 1950; *Komar*, 1979]. If there is barely any sediment exchange between the bed and the suspended sediment, then it is

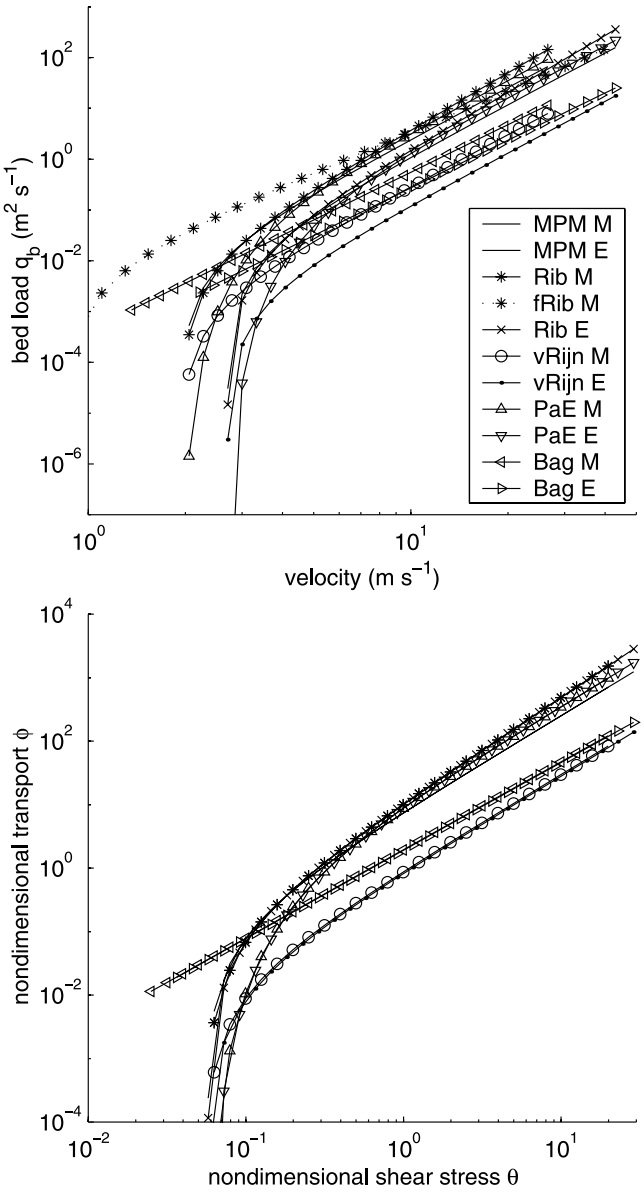

Figure 8. Comparison of bed load transport predictors. The differences span two orders of magnitude. Note that some predictors asymptotically go to zero transport near incipient motion, while others ignore this. The curves of Earth ("E") and Mars ("M") collapse in nondimensional space, even though the sediment density differs. "MPM": *Meyer-Peter and Mueller* [1948]; "Rib": *Ribberink* [1998]; "vRijn": *Van Rijn* [1984a]; *Kleinhans and van Rijn* [2002]; "PaE": *Parker et al.* [1982]; "Bag": *Bagnold* [1966]. The "fRib" is calculated with grain shear stress rather than total shear stress and only is larger for $u < 10$ m/s.

called wash load. Another characteristic of wash load is that it is limited by the amount of upstream supply [e.g., *Walling and Fang*, 2003], which makes comparison between different regions and planets very difficult. Aspects of wash load are discussed in section 6.

5.2. Bed Load Transport

[44] Common bed load sediment transport predictors are of the following nondimensional or a similar form [*Meyer-Peter and Mueller*, 1948; *Van Rijn*, 1984a; *Ribberink*, 1998; *Soulsby and Damgaard*, 2005]:

$$\phi_b = \alpha(\theta' - \theta_{cr})^{\beta} \tag{28}$$

where ϕ_b = nondimensional transport ("Einstein parameter"), in this case for bed load but in general defined as

$$\phi = \frac{q_{b\,or\,s}}{(Rg)^{1/2} D_{50}^{3/2}} \tag{29}$$

wherein $q_{b\ or\ s}$ = bed load or suspended load sediment transport rate (m^2 s^{-1}, cubic m per m width per second) excluding pore space, α = empirical constant of $O(1-10)$ and $\beta \approx 1.5$. The nondimensional shear stress and θ' = nondimensional shear stress related to grain friction only (equation (17)) or assuming plane bed with the total shear stress (equation (16)). Note that the total shear stress method is preferred here, because for the grain shear stress method the uncertainty of two friction equations is introduced whereas the total shear stress depends directly on measurable depth and slope of the channel. The assumption of plane bed must be checked with the Froude criterion for critical flow and the Shields criterion for upper stage plane bed (shown later).

[45] Consequently, the bed load transport rate depends on shear stress to the power of 1.5 or flow velocity to the power of 3, and near the beginning of motion (described by the Shields curve, equation (23)) the transport asymptotically goes to zero. The use of the nondimensional transport and shear stress parameters ensures that the functions are valid for different gravity, grain density and fluid density (Figure 8) [*Einstein*, 1950; *Bagnold*, 1966].

[46] The *Meyer-Peter and Mueller* [1948] predictor ("MPM") [also see *Kleinhans and van Rijn*, 2002] was derived from flume experiments with well-sorted gravel near the beginning of motion. The equation is

$$\phi_b = 8(\theta' - \theta_{cr})^{1.5} \tag{30}$$

The *Bagnold* [1966] predictor ("Bag") was based on energy considerations (stream power $\omega = u\tau$), and also depends on u^3. Bag does not contain the criterion for incipient motion. It contains a calibrated efficiency factor which is valid for the sand grain size range. It does not contain a correction for friction generated by bed forms which is a flaw for rivers on Earth. The equation is commonly written in dimensional form:

$$q_b = \frac{e_b \omega}{(\rho_s - \rho) g \cos S (\tan\varphi - \tan S)} \tag{31}$$

wherein e_b = transport efficiency factor approximated for $0.3 < u < 3$ m/s as [*Chadwick and Morfett*, 1993]

$$e_b = a \log 3.28u + b \tag{32}$$

where for $0.015 < D < 0.06$ (D in mm) $a = -0.012$ and $b = 0.15$, for $0.06 < D < 0.2$ $a = -0.013$ and $b = 0.145$, for $0.2 < D < 0.7$ $a = -0.016$ and $b = 0.139$, and for $D > 0.7$ $a = -0.028$ and $b = 0.135$. Furthermore, the angle of repose

$\tan\varphi = 0.7$ for $G^2 < 150$, $\tan\varphi = 0.374$ for $G^2 > 6000$, and $\tan\varphi = -0.236 \log G^2$ for $150 < G^2 < 6000$, wherein the Grain flow number

$$G^2 = \frac{\rho_s D^2 u^{*2}}{\rho 14 \nu^2} \tag{33}$$

The *Parker et al.* [1982] approximation to the Einstein equation (''PaE'') was developed for gravel transport in natural streams near the beginning of motion (without bed forms). The equation is

$$\phi_b = 11.2 \frac{(\theta' - \theta_{cr})^{4.5}}{\theta'^3} \tag{34}$$

The *Van Rijn* [1984a] predictor (''vRijn'') [also see *Kleinhans and van Rijn*, 2002] was derived from calibrated predictors of the saltating motion of sand particles. It forms a consistent set with the suspended load transport model of *Van Rijn* [1984b]. The bed load equation is

$$\phi_b = 0.1 \left(\frac{\theta' - \theta_{cr}}{\theta_{cr}} \right)^{1.5} D^{*-0.3} \tag{35}$$

The *Ribberink* [1998] predictor (''Rib'') was carefully calibrated on a large amount of data in currents, waves, combined flow, mostly sand but also gravel, and in conditions near the beginning of motion and far into the sheet flow range. The equation is

$$\phi_b = 11(\theta' - \theta_{cr})^{1.65} \tag{36}$$

Recently, *Soulsby and Damgaard* [2005] derived a bed load predictor from physics and calibrated this with a similar data set as *Ribberink* [1998]. The resulting equation is similar to that of *Ribberink* [1998] and will not be shown.

[47] Both bed load and suspended load transport were calculated for a range of Martian conditions. The grain size used here was $D_{50} = 0.1$ m (Table 1), the depth was varied between $2D_{90}$ and 900 m, the channel slope was kept constant at $S = 5 \times 10^{-3}$ and for flow roughness equation (13) was used. A check for the bed forms revealed that the bed is always planar which justifies the use of this roughness function.

[48] The differences between bed load predicted with the equations above span two orders of magnitude (Figure 8), even for conditions on Earth for which they were calibrated. The differences for the dimensional bed load transport for Earth and Mars are within a factor of two or three, while nearly collapsed on top of each other in nondimensional form. This indicates correct dimensional analysis which allows the use for different gravity and sediment densities. Upon close inspection the vRijn and Bag are smaller while the MPM, Rib and PaE are within a factor of two. The vRijn equation is sensitive to grain size through the D^* parameter but this was calibrated for sand only. Also the Bag was calibrated for fine sand only. Since Rib is calibrated for the largest mobilities and agrees well with other gravel bed predictors, this is favored herein.

5.3. Suspended Load Transport

[49] Two well-known suspended load predictors are given: the *Van Rijn* [1984b] (''vRijns'') and the *Bagnold* [1966] (''Bags''). A third well-known predictor for total load (sum of bed load and suspended load) is also compared here [*Engelund and Hansen*, 1967] (''EH''), because it was derived for suspension-dominated conditions. For clarity we start with the last, which was based on energy consideration and calibrated on flume experiments:

$$\phi_s = \frac{0.1}{f} \theta^{2.5} \tag{37}$$

wherein ϕ_s = nondimensional suspended load transport and f = Darcy-Weisbach coefficient related to total roughness. Consequently, the suspended load transport rate depends on shear stress (including form roughness) to the power of 2.5 or flow velocity to the power of 5, which is larger than for bed load. Also, the EH does not incorporate the criterion for incipient motion. The *Bagnold* [1966] equation is similar to that of bed load and is

$$q_s = \frac{e_s (1 - e_b)\omega}{(\rho_s - \rho) g \cos S \left[(w_s/u) - \tan S \right]} \tag{38}$$

wherein $e_s = 0.015$ efficiency factor for suspension.

[50] The *Van Rijn* [1984b] equation consists of a number of modules for different elements of the suspended load transport process. Basically, the suspended sediment transport load is calculated as the product of the vertical distributions of concentration and flow velocity between the top of the bed load layer and the water surface [*Einstein*, 1950]:

$$q_s = \int_a^h u_z c_z dz \tag{39}$$

where a = reference level at which the lowest concentration is calculated, taken at $a = k_s$, c_z and u_z are concentration and velocity at level z, respectively. The velocity profile is the well-known law of the wall for rough flow ($Re^* > 11.63$):

$$u_z = \frac{u_*}{\kappa} \ln \left[\frac{z}{0.033 k_s} \right] \tag{40}$$

where u_* = shear velocity and κ = von Kármán constant (0.4). The depth-averaged flow velocity is found at a height of $(1/e)h \approx 0.368h$, where h = water depth and e = Euler constant. The vertical concentration distribution can be described in many forms, of which the two following are common:

$$\frac{c_z}{c_a} = \left(\frac{a}{z} \right)^Z \tag{41}$$

$$\frac{c_z}{c_a} = \left(\frac{h - z}{z} \frac{a}{h - a} \right)^Z \tag{42}$$

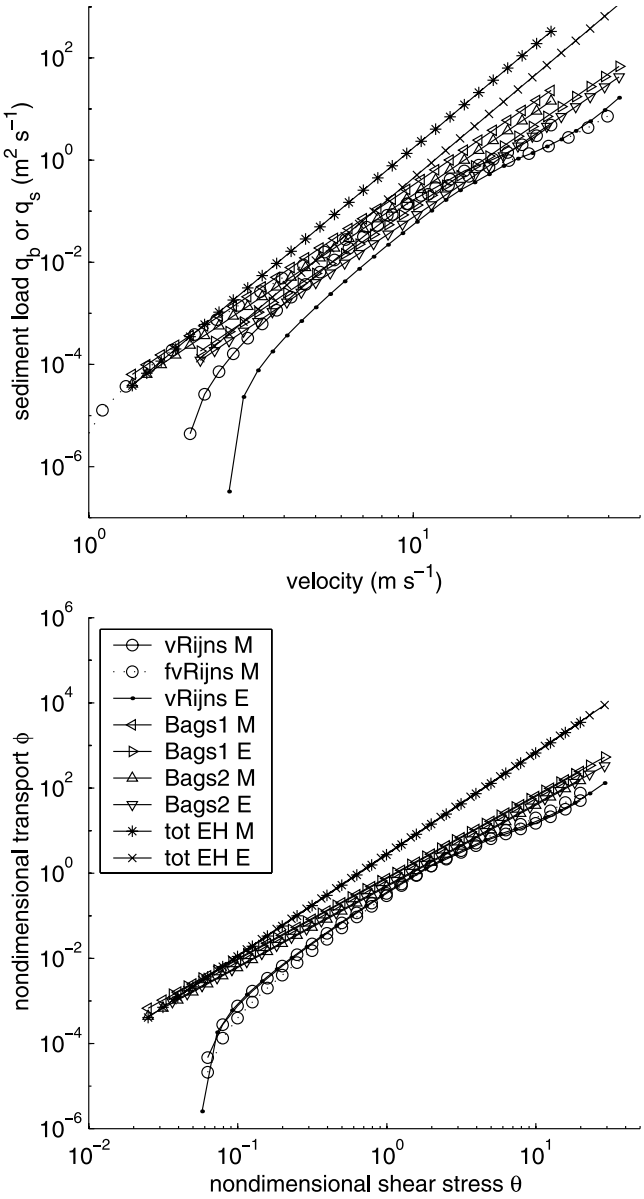

Figure 9. Comparison of suspended load transport predictors. The bed load predictors of *Van Rijn* [1984a] and *Bagnold* [1966] are given for comparison. As in bed load, the differences span two orders of magnitude. The curves of Earth (''E'') and Mars (''M'') collapse in nondimensional space, even though the sediment density differs. The *Bagnold* [1966] equation is given twice with the settling velocity functions of *Dietrich* [1982] and *Soulsby* [1997]. ''vRijn'': *Van Rijn* [1984b]; ''EH'': *Engelund and Hansen* [1967] for total transport. The ''fvRijn'' is calculated with grain shear stress rather than total shear stress and only is larger for $u < 10$ m/s.

where c_a is the reference concentration at height a and Z is the Rouse Suspension number given here as

$$Z = \psi + \frac{w_s}{\gamma \kappa u*} \tag{43}$$

in which w_s = settling velocity (here equation (25)), ψ = stratification correction at large concentrations (discussed in section 6) and γ = ratio of fluid and sediment mixing coefficient ($\gamma_{max} = 2$). The reference concentration is essentially the concentration of the bed load transport layer and therefore resembles equation (35):

$$c_a = 0.015 \frac{D_{50}}{a} \left(\frac{\theta' - \theta_{cr}}{\theta_{cr}} \right)^{1.5} D*^{-0.3} \tag{44}$$

where c_a is expressed in m^3/m^3 excluding pore space and obviously $c_a < c_0$ where $c_0 = (1 - \lambda)$ is the bed sediment concentration (m^3/m^3) depending on the porosity λ. The concentration and transport by weight is calculated by multiplying with the sediment density ρ_s. Note that the reference concentration depends on grain-related shear stress (τ' or θ') whereas the shape of the concentration profile depends on the total shear stress ($u*$). Alternative predictors for reference concentration are numerous in the literature. The depth-integration of suspended transport cannot be done analytically but must be done numerically. For practical purposes *Van Rijn* [1984b] developed an analytical approximation accurate within 25% which is used herein for simplicity:

$$q_s = Fuhc_a \tag{45}$$

where F is given as:

$$F = \frac{(a/h)^Z - (a/h)^{1.2}}{(1 - a/h)^Z (1.2 - Z)} \tag{46}$$

[51] The differences between suspended load predicted with the equations above span two orders of magnitude (Figure 9), even for conditions on Earth for which they were calibrated. The differences for the dimensional suspended load transport for Earth and Mars are within a factor of three, while nearly collapsed on top of each other in nondimensional form. This indicates correct dimensional analysis which allows the use for different gravity and sediment densities. Upon close inspection the Bags has a smaller power, yielding smaller rates at large velocities, whereas the EH has a larger slope. The vRijns gives intermediate transport rates. The Bags is slightly sensitive to the choice of the suspended settling velocity equation (1: equation (25) or 2: equation (27) in Figure 9) with a factor of two difference.

[52] The magnitude of suspended transport is the same as or smaller than that of bed load transport for the given conditions due to the large grain size (Figures 9 and 10). For the smaller Martian channels this means that the bed load transport is dominant, whereas suspended load transport becomes important in the larger channels with larger velocities.

[53] The sensitivity of the transport predictors to grain size varies widely (Figure 11). This was calculated by using a shear stress of $\tau' = 1000$ N/m^2 and slope of $S = 5 \times 10^{-3}$, computing velocity and water depth with the roughness predictor and then varying only the grain size. Except for the Bag bed load predictor, the transport rate decreases with increasing grain size. This result clearly

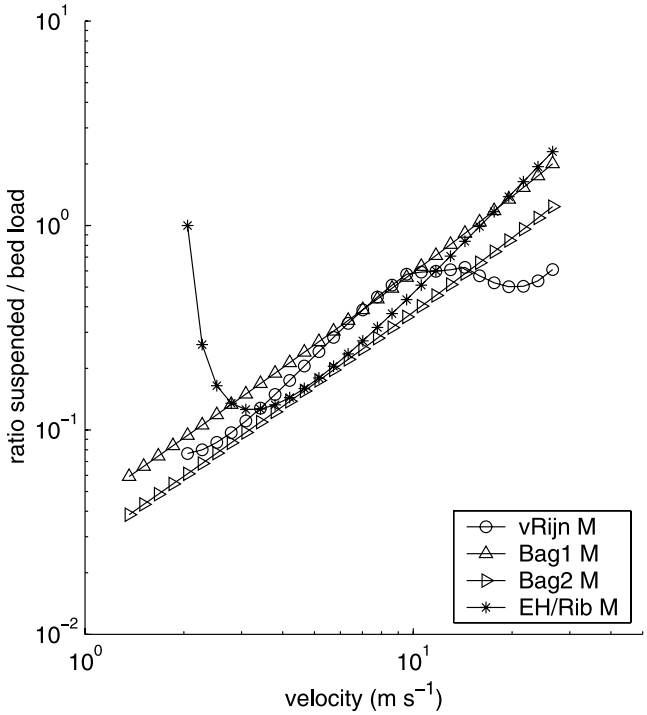

Figure 10. Ratio of suspended and bed load transport rates. Only for $u \gg 10$ the ratio becomes slightly larger than unity for the grain size (gravel!) and flow conditions representative for Martian channels. Note the effect of the criterion for incipient motion in the ratio of *Engelund and Hansen* [1967] and *Ribberink* [1998].

shows that a good description of the sediment is necessary for reliable sediment transport predictions, which may otherwise easily be an order of magnitude too large or small. In addition, for mixtures of grain sizes with a large standard deviation the sediment transport should be calculated for each grain size fraction and then summed to yield the total bed or suspended load transport rate [e.g., *Parker et al.*, 1982; *Kleinhans and van Rijn*, 2002; *Parker*, 2005; and references therein]. For the suspended load transport the largest effect is obviously in the settling velocity for the different grain sizes, and the finer sediment consequently will contribute more to the suspended transport rate. For both the bed load and the reference concentration there is a special sorting effect that must be accounted for: the fines hide in the lee of larger grains whereas the larger grains are more exposed to the flow than would be the case in a uniform sediment bed. This hiding-exposure effect thus leads to larger critical shear stress for the finer sediment and smaller critical shear stress for the coarser sediment. For unimodal sediment the critical shear stresses of all sizes may actually become the same, but for bimodal sediment (likely the case on Mars as argued in this paper) there remains a difference [*Parker et al.*, 1982; *Kleinhans and van Rijn*, 2002; *Parker*, 2005]. In short, sediment transport prediction with the *Ribberink* [1998] bed load predictor is recommended but the estimated uncertainty is at least an order of magnitude. Given the large uncertainty about the grain size distribution of Martian sediments the fractional approach is not further developed herein.

6. Hyperconcentrated Flow

[54] In large sediment concentrations the effective settling velocity of the grains is decreased due to the large concentration. The condition where large concentrations are present in the lower part of the flow is called stratification ($c <$ 0.15 or <15% of volume). The grains collide in the settling process and the downward movement of the grains enforces upward movement of the fluid, both of which hinder the settling. In addition, the shear stress, which is the sediment entraining force per unit area, increases due to the increased density of the water-sediment mixture. As a feedback, the turbulence that carries the suspension is damped to some extent. *Van Rijn* [1984b] calibrated an empirical stratification correction on flume experiments which is used in equation (44):

$$\gamma = 2.5\left(\frac{w_s}{u*}\right)^{0.8}\left(\frac{c_a}{c_0}\right)^{0.4} \tag{47}$$

[55] Extremely large concentrations (>0.15 or >15% of volume) are called hyperconcentrated flows. The hindered settling becomes dominant and the water-sediment mixture behaves as a pure liquid wherein the sediment is well mixed in the flow and the sediment concentration gradient above the bed is small. This condition occurs in the Yellow River but also in high-density turbidity currents at the ocean

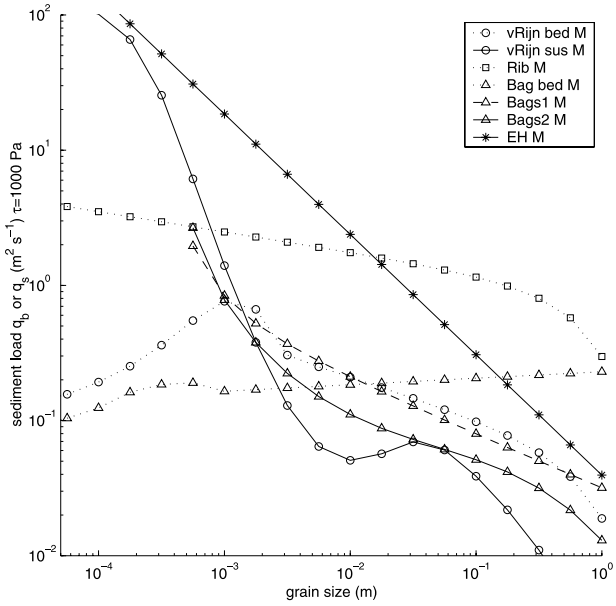

Figure 11. Sensitivity of transport predictors to grain size at a constant bed shear stress $\tau = 1000$ N/m^2. The bed load functions (stippled lines) reflect the shape of the Shields curve (upside down). The bed load function of *Bagnold* [1966] and the suspended load functions decrease with grain size due to the settling velocity increase. The Bags could not be calculated for $D_{50} < 0.7$ mm because the factor $[(w_s/u) - \tan S]$ in equation (38) becomes negative for these conditions.

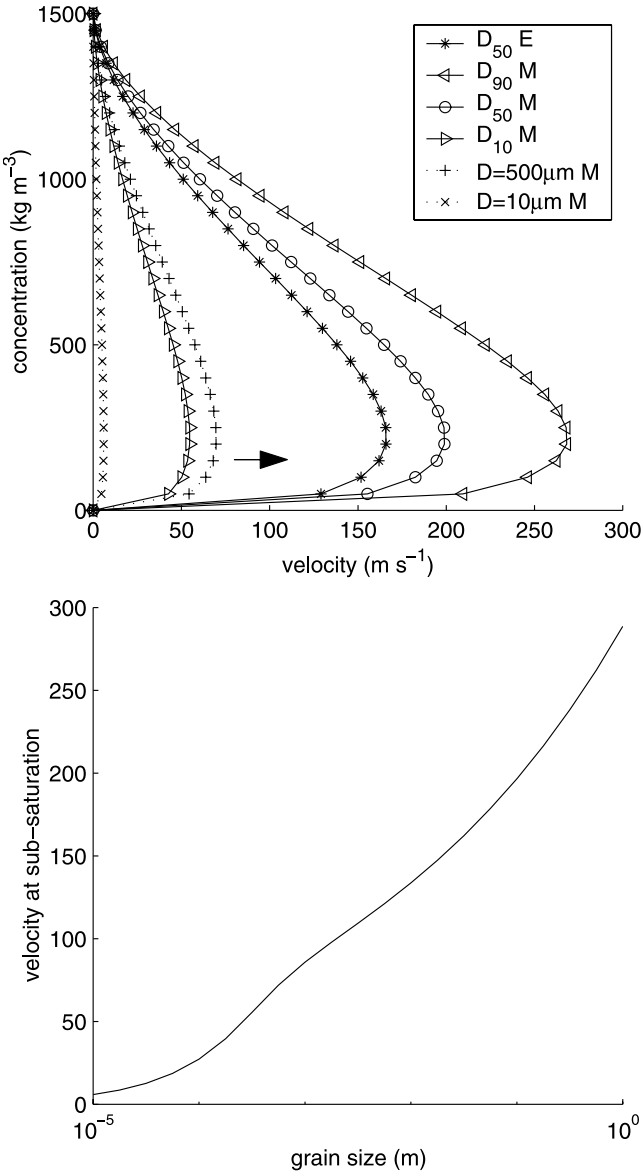

Figure 12. Wash load concentration as a function of velocity, and the velocity at sub-saturation (at the velocity peak in the top panel) versus grain size (bottom panel). Very large velocities are needed to get hyperconcentrations of gravel by entrainment from the bed.

margins on Earth. The maximum concentration is about $c_{\max} \approx 1000$ kg/m^3 but it depends on the sediment grain size distribution: poorly sorted sediment (with a range of grain sizes) may reach maximum concentrations of $c_{\max} \approx 1500$ kg/m^3 as found in flume experiments (L. Van Rijn, A unified view on sediment transport by currents and waves: part 3, Suspended transport, submitted to Journal of Hydraulic Engineering, 2005; hereinafter referred to as Van Rijn, submitted manuscript, 2005). This condition is similar to wash load in two respects: there is barely any interaction between the sediment in suspension and in the bed, and the sediment is mixed well throughout the water depth. Wash load, on the other hand, may also consist of very small concentrations of sediment finer than in the bed. The hyperconcentration may increase the effective density of the flow and hence the shear stress, leading to somewhat larger bed load transport rates but this can be neglected here.

[56] *Bagnold* [1966] and Van Rijn (submitted manuscript, 2005) based the suspension on the balance between the energy required to keep the sediment load in suspension and the energy dissipated by the transport of sediment. The energy to keep the sediment in suspension is

$$E_s = Rghcw_e \tag{48}$$

where w_e = effective sediment fall velocity including the effect of hindered settling. The settling velocity is corrected for hindered settling by

$$w_e = \left(1 - \frac{c}{c_{\max}}\right)^5 w_s \tag{49}$$

where w_s = settling velocity in clear water (equation (25)). The energy dissipated by the flow in transporting the sediment is

$$E_d = e_s \tau u \tag{50}$$

wherein $e_s = 0.015$ is the suspended sediment transport efficiency factor also used in equation (38) and

$$\tau = \rho_m f_m u^2 \tag{51}$$

wherein ρ_m = mixture density and $f_m = 7.85 \times 10^{-3}$ roughness coefficient for hyperconcentrated flow. When E_s and E_d are in balance the sediment concentration is obtained:

$$c = \rho_s K(1 + \alpha c)\frac{u^3}{ghw_e} \tag{52}$$

wherein $K = (e_s f_m)/(8R)$ and $\alpha = R/\rho_s$ (Van Rijn, submitted manuscript, 2005). The relation can now be expressed in nondimensional form as

$$\frac{u^3}{ghw_s} = \frac{c}{\rho_s K(1 + \alpha c)}\left(1 - \frac{c}{c_{\max}}\right)^5 \tag{53}$$

Solving this equation yields two concentrations for each velocity (Figure 12). The concentration at the maximum velocity is called sub-saturation. Larger concentrations are called hyperconcentrations.

[57] The point of Figure 12 is that the velocity at sub-saturation must be exceeded for hyperconcentrated flow to occur by entrainment of sediment from the bed. For the assumed D_{50} of the Martian soil this velocity is about $u \approx 200$ m/s, which is an order of magnitude larger than predicted even for the largest Martian channels. It is not unlikely, however, for the sandy part of the soil for which a velocity of $u \approx 65$ m/s must be exceeded for hyperconcentration. In other words, it is unlikely that hyperconcentrations occur for the Martian channel sediment except for the fine mode of the grain size distribution. This mode then behaves independently from the coarse mode, which will be transported as bed load or suspended load.

[58] There may be exceptional conditions that cause hyperconcentration for the gravel and cobbles. It involves en masse supply of sediment to the flow, which may then become a hyperconcentration (upper part of Figure 12). This is unlikely in valleys created by groundwater sapping processes, which are relatively slow, but might have occurred in the largest catastrophic outflow channels if the melting process was violently initiated by volcanism. However, even in this case the channels were not formed at first, which implies that the flow was not concentrated yet.

7. Discussion

7.1. Timescale of Channel and Delta Formation

[59] The minimum timescale of formation of a channel or delta can be estimated as

$$T_s = \frac{V_s}{(1-\lambda)Q_s} \tag{54}$$

wherein V_s = volume of eroded (from a channel) or deposited (in a delta) sediment including pores and $Q_s = (q_b + q_s)W_s$ with W_s = width of that part of the channel floor that transports the sediment. The porosity of the sediment (λ)is well constrained between 0.2–0.4 and the transporting channel width is probably in between 0.5–1 of the full channel width W. With the high quality digital elevation models of the Mars Express HRSC and the MOLA [*Zuber et al.*, 1992] for larger channels the volume of the eroded or deposited sediment is now better constrained, so the largest uncertainty is likely in the sediment transport prediction. The timescale of the flow can also be calculated if the source volume of water is known (as in the Ma'adim Vallis case) or assumed (for example, by using an estimated volume of the northern ocean on Mars). This timescale is written as

$$T_w = \frac{V_w}{Q} \tag{55}$$

where the subscript w is for water.

[60] The timescale of formation is a minimum, because the flow magnitude derived from existing channels ignores the fact that these channels are the end products of the process. Even if the upstream flow discharge was constant and as large as calculated from the channel morphology, then the channels must have started as shallow, poorly confined channels with much smaller shear stresses and consequently much smaller sediment transport rates. Especially for the catastrophic conditions on Mars, the concept of a representative channel-forming bankfull discharge sensu [*Wolman and Miller*, 1960] is not of much use. This concept was devised for the conditions on Earth, where, for example, in an idealized situation equilibrium river channels move over slowly aggrading delta plains. Such moving rivers may maintain remarkable constant geometries over large distances. Nevertheless some rough scaling between Martian channel dimensions and the flow discharge is of course expected, which renders a rough application of the proposed equations feasible albeit with a large uncertainty [see also *Wilson et al.*, 2004].

[61] The uncertainty of sediment transport prediction obviously has large consequences for the calculation of the timescale of formation of channels and deltas. Specifically, the prediction of hydraulic roughness and sediment transport are very uncertain. Many models are based on proper nondimensional analysis but the weakness is in the calibration to a limited data set. The sediment transport models for gravel are not calibrated for high energy conditions while the models for high energy conditions apply to sand only. Despite all uncertainties the general trends are clear. Only if sediment mixed with water is supplied to a channel in large quantities and in a catastrophic manner, then a hyperconcentrated flow may commence, or, in extreme cases, a debris flow may be initiated. Alternatively, if the flow velocity is large enough (depending on the grain size), then enough sediment may be entrained from a noncohesive channel bed to generate a hyperconcentrated flow. If the flow is not hyperconcentrated then the concentrations are orders of magnitude smaller.

[62] Moreover, channel-forming discharges on Earth occur roughly for about 5% of the time [*Parker*, 2005]. The timescale obtained above should therefore be multiplied with at least a factor of 20. This number cannot be applied straightforwardly to Mars because the nature of the various channels is very different [*Sharp and Malin*, 1975]. The largest channels are clearly catastrophic and their source areas show collapse features [*Sharp and Malin*, 1975; *Carr*, 1996]. Smaller channels often have groundwater sapping valleys upstream, which indicates a more moderate discharge regime [*Sharp and Malin*, 1975; *Laity and Malin*, 1985]. Observations and flume experiments on Earth clearly indicate that sapping channel networks react to precipitation but in a slower and more damped manner than overland flow networks [*Laity and Malin*, 1985; *Howard et al.*, 1988; *Dunne*, 1990]. The response also depends on the porosity of the substrate, which depends on the grain size of the sediment and on fracturing. In short, given the present lack of knowledge of the substrate and of the past hydrological conditions, an estimate of the time in between groundwater reloadings is speculative. So, if $T_s > T_w$ as will be shown for many examples (see also section 7.5), then it is an inevitable outcome that reloading took place, and that the true timescale of formation may easily be a factor of 10–1000 larger than the water or sediment transport timescales calculated herein.

[63] In addition, the application of the sediment transport predictors imply that the erodible material is loose and noncohesive. If the material is cohesive, then the sediment transport rates are much smaller and are not in the hyperconcentration range. This condition is called detachment- or supply-limited, contrary to the capacity-limited condition where erodible sediment is present and the flow is the limiting factor for the sediment transport rate. In the detachment-limited case a limited amount of bed load transport will lead to the largest rate of rock abrasion [e.g., *Sklar and Dietrich*, 2004, and references therein]. An indication for capacity-limited conditions is the presence of a rather smooth and straight or slightly curved channel bed profile. Heterogeneities in the bedrock would lead to scour holes, teardrop-shaped islands, sudden jumps, etc. (excluding fluvial bars). Many channels indeed have such

features which merits further work on bedrock or regolith erosion.

[64] A poorly understood problem is the initiation of water and sediment outflow. The source of the water may be groundwater sapping, which depends on pore space and ground water flow, catastrophic lake overflow as for Ma'adim Vallis [*Cabrol et al.*, 1996; *Irwin et al.*, 2002] or catastrophic melt water release and regolith collapse as upstream of the largest outflow channels [*Williams et al.*, 2000], which again depends on pore space. Channels with upstream sapping valleys are generally smaller, which, together with the more durative nature of the sapping process [*Howard et al.*, 1988] may lead to channel dimensions that are nearly in equilibrium with the flow discharge regime. It is very likely that the sediment transport in these channels is dominated by bed load as described by the equations in this paper. Yet again the groundwater reloading time depends on the hydrological conditions of early Mars.

[65] The possibility of the catastrophic melt water release and regolith collapse mechanism was studied in more detail by *Wilson and Mouginis-Mark* [2003], *Wilson and Head* [2004], and *Head et al.* [2003]. They suggest that repeated subsurface volcanic dike and sill emplacement caused surface and cryosphere fractures and possibly explosive volcanism, through which pressurized groundwater from beneath the cryosphere was released. In this explosive volcanism phase, sand-sized particles would have been ejected and mud flows (lahars) would be generated. Only in a later stage the volcanic heating of the regions adjacent to the dikes caused melting, valley wall collapse and fluvial erosion. Although the valleys could harbor large catastrophic discharges, the groundwater reservoirs would probably not allow such large discharges unless a large-scale interconnected fracture system exists [*Head et al.*, 2003; *Wilson and Mouginis-Mark*, 2003]. The implications of their theory and observations are that hyperconcentrated flows (lahars) would have been generated but only with a limited outflow length, but later moderate (not bankfull and not hyperconcentrated) fluvial activity would have taken place. Interestingly, the ejecta and mud flow deposits would form a source of sand-sized sediment in addition to the poorly sorted rocky sediment derived from valley wall collapse and local debris flows. This is in agreement with the subsequent moderate and low-concentration fluvial outflow scenario for excavating most of the channel as proposed in this paper.

7.2. Tell-Tale Delta Morphologies

[66] The morphology of the sediment deposits, likely in the form of deltas, is indicative of the formation process, and thus partly related to the sediment mobility in the feeder channel. There are various classifications for deltas, commonly based on environmental parameters and grain size [e.g., *Orton and Reading*, 1993; *Postma*, 1995; *Cabrol and Grin*, 2001]. The mobility of the sediment strongly determines the general delta morphology.

[67] Barely mobile sediment transported as bed load will form Gilbert-type deltas when debouching into a basin. These have a top slope equal to or smaller than the feeder channel slope due to flow divergence, and foresets near the angle of repose created by avalanching of sediment which was deposited at the basin margin due to the sudden flow expansion. The height of the foresets (and hence the thickness of the delta) depends on the basin depth. Consequently, a condition for the formation of a Gilbert-type delta is accommodation space in the basin. In general, a (crater) lake is a perfect sediment trap. Gilbert-type deltas are therefore ideal for sediment transport and timescale studies on Mars. Alluvial fans, which are similar to the Gilbert-type deltas except for their downstream boundary conditions (empty rather than water-filled basin) [*Parker*, 1999], may loose a small portion of their sediment if a channel continues downstream of the fan, but for practical purposes an alluvial fan is also a nearly perfect sediment trap.

[68] On the other end of the spectrum is the deposit generated by highly mobile sediment. A hyperconcentrated flow debouching into a basin may cause a hyperpycnal plume, or density current, over the basin floor, or, alternatively, a hypopycnal plume of small particles near the surface [*Orton and Reading*, 1993]. The hyperpycnal plume results in a low-sloping deposit and possibly submarine channels as in the case of, e.g., the Amazon fan [*Pirmez and Imran*, 2003]. The hypopycnal plume also results in a low-sloping deposit. Contrary to the Gilbert-type delta, the result of highly mobile sediment is a low-sloping delta or even amorphous (wash load) deposit ranging far into the basin. Possibly the fines may block the pore spaces of the coarser material which increases the effect of hyperconcentration. In that case the coarse sediment would be suspended more so that no Gilbert-type delta could be formed. This process is, however, poorly understood.

[69] In between these two extremes there is a range of possible delta morphologies depending on the conditions, but also on the sediment grain size distribution. Two cases are discussed: a bimodal sediment mixture with fine and coarse sediment and no grades in between, and a unimodal mixture with grains present over the whole range of sizes. In the bimodal sediment case, the fines are transported in wash load or even as a hyperconcentrated flow whereas the coarse parts are transported as bed load, possibly with some suspension. The wash load will barely affect the bed load, so these two sediment modes will behave relatively independently. When debouching into a basin, the coarse load will generate a Gilbert-type deposit, while the fines will deposit as a toe-set at the bottom of the basin downstream of the delta. Since the largest deposition occurs just downstream of the delta, the toe deposit may have an exponential profile. If for the unimodal mixture hyperconcentrated flow occurs at all, then this may likely drag most available sizes into suspension. The resulting delta is therefore probably more like that generated by the high sediment mobility flows as discussed above and a lower-sloping Gilbert-type delta with a gradual transition between steeper foreset and shallower toe deposit.

[70] *Hauber et al.* [2005] studied crater-lake deltas in Xanthe Terra, which show the morphology of the bed load-dominated and bimodal sediment delta cases. The Nanedi Vallis delta is a well-preserved bed load-dominated Gilbert-type delta strikingly similar to laboratory analogue deltas. The Hypanis Vallis delta is clearly a Gilbert-type delta but with a considerable toeset deposit [*Hauber et al.*, 2005], although part of the toeset is probably windblown material deposited later. A few deltas described by *Ori and Mosangini* [1998] and *Cabrol and Grin* [2001] also clearly

show Gilbert-type features combined with mud-like emplacements by wash load deposition. The mesas in the Gusev Crater just downstream of Ma'adim Vallis suggest the former presence of a Gilbert-type delta [*Kleinhans et al.*, 2005]. Crater modelling indicates infilling by additional sediment downstream of the assumed delta relics [*Cabrol et al.*, 1996; *Irwin et al.*, 2004; *Zegers et al.*, 2005]. This infilling may either have occurred by a hyperconcentrated flow in an earlier phase than the formation of the delta, or simultaneously if the sediment is sufficiently bimodal. In fact, the wash load sediment would travel downstream at the same velocity as the water, whereas the bed load would travel much slower, so the lowest deposit, underlying the coarse-grained delta, may well be fine material. The Sabrina Vallis delta shows more channel-like protuberances at the basin margin, indicating a larger sediment mobility, but nevertheless there is a high-angle slope like that of foresets [*Hauber et al.*, 2005]. The fan delta in the Holden NE crater [*Malin and Edgett*, 2003] has a similar morphology. The presence of channels on the delta top does not necessary imply that it is an alluvial fan of which the downstream end was eroded by some process; alluvial processes also take place on the top of Gilbert-type fan deltas.

7.3. Debris Flow Hypothesis

[71] *Nummedal and Prior* [1981] and *Tanaka* [1999] suggested that the largest outflow channels on Mars were created by large debris flows. If that is the case, then the present paper describes the wrong mechanism for sediment transport. When the volume concentration becomes larger than ≈40%, the behavior of the fluid changes to non-Newtonian [*Hungr*, 1995; *Iverson*, 1997]. This is for example the case in lahars [*Russell and Head*, 2003], dense turbidity currents [*Baas et al.*, 2004] and debris flows [*Iverson*, 1997; *Rickenmann*, 1999]. As a consequence of the non-Newtonian behavior, the run-out lengths of the flows are much shorter than those of fluvial channels [*Iverson*, 1997]. The question is whether conditions occurred on Mars that allowed the formation of large debris flows with run-out lengths large enough to explain the mega-outflow channels. Submarine turbidity currents may be relevant for the deposits on the northern hemisphere of Mars and may have originated from hyperconcentrated flow or debris flow into the ocean. Turbidity currents are, however, not relevant for the flow in the channels that are the focus of this paper (or it must be assumed that the planet was completely covered by a shallow sea which is not a realistic hypothesis).

[72] It is entirely unlikely that the long, relatively small channels such as Nanedi Vallis and other sapping valleys on Mars were generated by channelized debris flows. The possibility of a debris flow origin is therefore only relevant for the largest channels. Debris flows are not the scope of this paper, so the discussion is kept short and focussed on run-out length because at least the length of the channels on Mars should be explained by the mechanism. In the small (sapping) valleys, the flow and sediment transport equations given in this paper do apply (also see the examples in section 7). Debris flows may occur in the walls of the channels but that is not the point here.

[73] The run-out lengths of debris flows depend on the water content and on the presence of fines (especially cohesive material) in the pore space of coarser material. The run-out length L (in m) of debris flows has been related to the descent height H (in m) of the source of sediment from which the flow is generated, and to the source sediment volume M (in m^3) [*Hungr*, 1995; *Iverson*, 1997; *Rickenmann*, 1999]. In addition, the volume of the flows on Earth is approximately the same as the source volume of sediment, which indicates that entrainment of sediment from the bottom of the flow is not important. The implication is that the source area of a large debris flow on Mars should have a high elevation and a large volume. An alternative to the high elevation would be high pressure (expressed as a height or "hydraulic head") in the source area.

[74] The run-out lengths for debris flows on Earth are tabulated in *Iverson* [1997] and *Rickenmann* [1999]. A simple equation to predict the run-out lengths is [*Rickenmann*, 1999, equation (22)]

$$L = 30(MH)^{1/4} \tag{56}$$

This equation covers experimental landslides of about 100 m length to landslides of 120 km length which are the largest on Earth. Rock falls and other dry granular flows have run-out lengths an order of magnitude smaller. Of course this simple equation has many limitations, and more sophisticated physical models are necessary for more detailed predictions of individual debris flows [*Iverson*, 1997]. For example, the run-out length is also affected by the grain size distribution of the sediment, channelling of the debris flow and gravity.

[75] The debris flow hypothesis for mega-outflow channels on Mars is tested by computing the order of magnitude of run-out length with the above equation. Simud Vallis and Tiu Vallis have lengths of the order of 1000 km, and the fluidization and erosion depth at the source area is of the order of 1 km [*Tanaka*, 1999]. From the above equation it follows that a source volume of 1×10^6 km^3 is needed to have an outflow length of the same length as the channel length, or, given the erosion depth, a source area of 1000×1000 km^3. Note that the sides of this area are as long as the channel. The real source area is about an order of magnitude smaller. This calculation may be crude, but the point is that an impossible volume of material has to be fluidized and mobilized to initiate a debris flow that is capable of creating the mega-outflow channels. This indicates that it is unlikely that the mega-outflow channels were created by debris flows. We will now return to the fluvial mechanism and calculate flow, sediment transport and minimum timescales of formation for a number of examples.

7.4. Examples of Flow and Sediment Transport in Martian Channels

[76] Equations (2), (7), (9), (13), (3), and (1) and the preferred sediment grain size distribution (Table 1) are applied to a number of example channels on Mars and Earth (Table 2). The flow velocity varies between a factor of 1–4 for different roughness assumptions. In general, the velocities with the new roughness predictor (equation (13)) are smaller than previous estimates. The large velocities for the *Baker* [2001] data are due to the incorrect slopes.

Table 2. Examples of Flow Reconstructions for Catastrophic Channels on Earth and Mars for Existing Data Sets

Name	Width, m	Depth, m	Slope, –	D_{90}, m	Volume, km^3	Prev. Q, 10^6m^3/s	Prev. u, m/s	$u_{n=0.0545}$, m/s	u Equation (9), m/s	u Equation (13), m/s	Q, 10^6m^3/s	T_w, yr
Missoula Flood (Rathdrum)[a]	6000	150	0.01	0.6		20	22.2	50.1	64.3	21.6	19	
Altai Flooding (Chuja)[a]	2500	400	0.01	0.6		20	20	82.8	103.9	30.2	30	
Jokulsa a Fjollum[a]	10000	10	0.001	0.125		0.7	7	2.7	4.5	3.6	0.36	
Mangala Vallis[a]	14000	500	0.003	0.6		20	2.9	60.5	46.1	17.2	120	
Maja Vallis[a]	80000	100	0.02	0.6		300	37.5	55.8	44.5	13.3	106	
Ares Vallis[a]	25000	1000	0.005	0.6		500	20	123.3	90.9	26.2	655	
Kasei Valles[a]	80000	1300	0.01	0.6	14	2000	19.2	213.9	155.2	35.2	3661	0.1
Kasei Valles old[b]	83000	374	0.001	0.6	14	2000	64.4	29.9	23	12.2	379	1.2
North Kasei Valles[b]	4400	93	0.002	0.6	14	10	24.4	16.4	13.1	7.5	3.07	145
Kasei Valles[b]	4500	22	0.0002	0.6	14	0.2	2	2	1.6	2.4	0.24	1850
Ma'adim Vallis[c]	4000	75	0.004	0.6	0.174	5	16.7	20.1	16.1	8	2.4	2.3
Nanedi Valles[d]	744	45	0.0037	0.6				13.1	10.4	6.1	0.2	
Sabrina Vallis[d]	575	25	0.0082	0.6				13.4	10.6	5.7	0.08	
Hypanis Valles[d]	750	28	0.0098	0.6				16	12.6	6.2	0.13	
Mackenzie Delta[e]	450	8	0.00003	0.0001		0.004	1	0.4	1.5	1	0.0036	
Rhine delta[f]	500	4	0.002	0.01		0.003	1.5	2	5.1	2.4	0.0048	
Laboratory N9[g]	0.075	0.011	0.014	0.005			0.35	0.09	0.17	0.24	1.98×10^{-10}	

[a] *Baker* [2002].
[b] *Williams et al.* [2000].
[c] *Irwin et al.* [2004]; lake volume from *Irwin et al.* [2002].
[d] *Hauber et al.* [2005].
[e] *Hill et al.* [2001].
[f] *Berendsen and Stouthamer* [2000].
[g] *Kleinhans* [2005a].

[77] Concerning the possible presence of bed forms the Froude numbers are ambivalent (Table 3) due to the uncertainty in hydraulic roughness. When Fr is calculated from equation (9), they are near unity indicating plane bed conditions. However, when equation (13) is used the lower numbers indicate subcritical flow potentially with bed forms. However, the Shields numbers indicate plane bed except for one case, which means that the bed will be plane even if the flow is not supercritical.

[78] The timescale T_w is derived from the northern ocean volume [*Head et al.*, 1999] for the Kasei Valles and for Ma'adim Vallis from the volume of the upstream lake [*Irwin et al.*, 2002]. Given that more outflow channels were probably active when Kasei Valles flooded, this timescale may be overestimated, but Kasei Valles was the largest channel and the order of magnitude could be correct. If a D_{90} = 0.209 m were used as by *Wilson et al.* [2004], then the discharges increase 5–10% for equation (9) and decrease 5–10% for equation (13).

[79] For the Kasei Valles the values clearly indicate that for the newer channel dimension estimates [*Williams et al.*, 2000] the ocean volume would have been filled within a few thousand years, assuming constant inflow (which is probably not the case). Given that Kasei Valles is one of the largest catastrophic outflow channels, this is still a rather long time. It either indicates wet periods for

Table 3. Examples of Sediment Transport Computations for Channels on Earth and Mars (in Table 2)[a]

Name	D_{50}, m	θ_{tot}	Fr Equation (9)	Fr Equation (13)	V_{delta}, km^3	$V_{channel}$, km^3	$q_{tot,Bag}$, m^2/s	$q_{b,Rib}$, m^2/s	$q_{tot,A44\%}$, m^2/s	$T_{s,true}$, yr	$T_{s,delta}$, yr	$T_{s,channel}$, yr	$T_{s,chan44\%}$, yr
Kasei Valles old[b]	0.1	1.54	0.62	0.33		904000	0.8	2	2008			112	0.112
North Kasei Valles[b]	0.1	0.74	0.7	0.4		904000	0.21	0.57	307			7429	13.8
Kasei Valles[b]	0.1	0.02	0.18	0.26		904000	0.0014	0	23				180
Ma'adim Vallis[c]	0.1	1.2	0.96	0.48	540	14000	0.36	1.3	264		2.1	55	0.273
Nanedi Valles[d]	0.1	0.62	0.8	0.47	1.15	3.74	0.13	0.41	121		0.08	0.25	0.001
Sabrina Vallis[d]	0.1	0.79	1.1	0.59	9.4	29	0.16	0.62	63		0.54	1.68	0.017
Hypanis Valles[d]	0.1	1.06	1.23	0.61	150	850	0.24	1.1	76		3.7	21	0.31
Mackenzie Delta[e]	0.00001	8.49	0.17	0.11	434		0.073	0.000085	3	2400	5446		
Rhine delta[f]	0.001	3.28	0.82	0.39	30		0.0068	0.0182	4	3500	1359		
Laboratory N9[g]	0.001	0.05	0.5	0.72	3.8×10^{-12}		0	0.000034	0	0.00002	0.00003		

[a] All computations were done with the grain size estimates from this paper and assuming continuous discharge (no flow intermittency). The two timescales T_s are derived from the eroded valley volumes (including fines) and deposited delta volumes (only gravel and cobbles), respectively (porosity λ = 0.35). The third T_s is assuming the maximum sediment concentration in the water (c_{max} = 1500 kg/m^3 $\approx$ 0.44) assuming that it consists of fines (sand and silt) only.
[b] *Williams et al.* [2000].
[c] *Irwin et al.* [2004]; delta volume from *Zegers et al.* [2005].
[d] *Hauber et al.* [2005]; not the main Nanedi Valles but a side valley.
[e] *Hill et al.* [2001].
[f] *Berendsen and Stouthamer* [2000].
[g] *Kleinhans* [2005a].

10,000–1,000,000 years, or that an early stage of Kasei Valles was much larger than the later stage channels described by *Williams et al.* [2000].

[80] The sediment transport computations were done with equations (16), (31), (36), and (54) and for the assumption of maximum sediment concentration in the water ($c_{max} \approx 0.44$ which means that about 1500 kg of sediment is suspended in 1 m^3 of fluid) assuming that it consists of fines (sand and silt) only (Table 3). The total sediment transport rate of the *Bagnold* [1966] bed load and suspended load is usually smaller than the bed load rate predicted with *Ribberink* [1998], which is preferred herein and used for the timescales. Both are orders of magnitude smaller than for the assumption of maximum hyperconcentration.

[81] The sediment timescales T_s are derived from the eroded volumes of channels, deposited volumes in the deltas and *Ribberink* [1998] or the hyperconcentration computation. The assumed porosity of eroded and deposited sediment is $\lambda = 0.35$. These estimates represent scenarios of bed load transport only and hyperconcentration flow for the fines. The timescales differ orders of magnitude. Speculating, if the hyperconcentration was limited to the fine sediment only, then the truth is probably nearer to the bed load transport scenario, because the fine sediment supplied to the channel and leading to hyperconcentration would depend on the total fluid and sediment feed rate to the channel from collapse or sapping processes. The fines would rapidly be depleted from the sediment available for transport at a certain time, whereupon the process is dominated by bed load transport.

[82] As a check, the sediment timescales were also calculated for two extremely different deltas on Earth: the large fine-grained Mackenzie delta in Alaska [*Hill et al.*, 2001], the sandy Rhine delta in the Netherlands [*Berendsen and Stouthamer*, 2000] and a small coarse-grained laboratory delta [*Kleinhans*, 2005a]. The intermittency of the given discharge is assumed to be 5% [*Parker*, 2005]. For these cases the calculated timescale is within a factor three of the true timescale despite the simplified approach of this paper and neglecting sediment loss due to wave reworking or laboratory scale effects. Given the fine channel sediment of the Mackenzie river, the *Bagnold* [1966] predictor for both suspended and bed load transport is used for the timescale of these two rivers. The calculated and real timescale of deltas on Earth could easily be matched by adapting the intermittency, which is taken here as a constant but in reality depends on the climate and hinterland characteristics (but see section 7.5).

7.5. Implications

[83] Two hypothetical implications of the above will be discussed: (1) The sediment derived from the highlands is bimodal with gravel and cobbles on the one hand and sand and silt on the other. (2) During the formation of Gilbert-type crater lake deltas a number of aquifer reloadings were necessary.

[84] The presence of Gilbert-type deltas implies low mobility sediment transport in the feeder channels. Given the dimensions of the channels and the flow reconstruction above, this implies gravel and cobble sediment. In many cases, there is also a toe deposit with a distinct break between delta foreset and toeset. This implies the presence of a much finer sediment mode in the upstream sediment supply. This observation agrees with lander observations of gravel and cobble sized sediments mostly between 0.01–1 m [*Golombek et al.*, 2003], but, notably, also sand of 0.1–0.8 mm [*Fenton et al.*, 2003; *Grotzinger and Athena Science Team*, 2004], and the presence of atmospheric dust of a few μm. As discussed in section 3, the rock size distributions strongly undersample the finer sediments. The bimodal nature of the sediment implies that a coarse-grained deposit could be present under the fine sediment in Chryse Planitia as also suggested by *Ivanov and Head* [2001].

[85] There are three indicative constraints on the ratio of the coarse and fine mode in the sediment. The first is that the main body of deposited sediment is probably fine sediment on the bed of the ancient ocean on Mars [*Ivanov and Head*, 2001]. The second is that a number of Gilbert-type deltas have only one-third of the volume of the eroded upstream channels [*Hauber et al.*, 2005; *Kleinhans et al.*, 2005], even though these deltas are "perfect" sediment traps. This indicates that only one third of the eroded sediment was coarse-grained (and was trapped) and the rest must have been fines that were deposited initially below the Gilbert delta and later downstream of the delta, or washed out through the overflow of such crater lakes. The third is that the pore space of the megaregolith is constrained in a narrow range. On the one hand, the largest possible pore space for clast-supported angular gravel is about 40% and for rounded, poorly sorted sediment about 25%, independent of mean grain size [*Allen*, 1984]. Groundwater sapping is most effective in sediment with large pore space and it is not likely that the regolith was matrix-supported. A portion of the pores will therefore have been filled with fine sediment. For collapse upon melting to occur, the regolith must contain water and possibly CO_2, which can have been present in the pores of the fine sediment which would be between 25–40%. In short, the sediment would be composed of one-third fines and two-thirds coarse sediment. However, it is unknown how much in situ weathering of the coarse sediment took place, which would increase the portion of fines. The generation of fines in the transport process is not very effective in suspension compared to the much more abrasive and long-duration bed load. Concluding, it is not unreasonable to assume roughly equal portions of fines and coarse material transported by the channels and deposited in crater lakes and the ocean. This would explain the mismatch between delta and channel volumes.

[86] For the formation of a delta, two timescales are important: one is the minimum formation timescale from sediment transport (T_s), and the other is the time (T_w) after which the source of the water is depleted and the source has been reloaded. If $T_w < T_s$ then reloading of the upstream water source is necessary to explain the existence of the delta. Since Gilbert-type deltas were formed in low mobility conditions, the volume transport rate of sediment is orders of magnitude smaller than that of water, except for the wash load which is at best half the sediment volume. This implies that the pore water released in one sapping or catastrophic melting event is certainly not enough to create the delta, so groundwater reloading must have taken place.

[87] Interestingly, also the large lake upstream of Ma'adim Vallis [*Irwin et al.*, 2002] must have reloaded (see

Tables 2 and 3), contrary to the assertion by *Irwin et al.* [2004], if the mesas in the Gusev Crater are indeed the remains of a Gilbert-type delta [*Zegers et al.*, 2005]. *Irwin et al.* [2004] based their computations on the false assumption that the sediment concentration was 40% of the volume of the flow, in which case the whole Ma'adim Vallis could have been eroded in one lake overflow event, of which the volume was estimated from MOLA topography. However, if the sediment was mobile enough for hyperconcentration then a Gilbert-type delta would probably not have formed. Given the present findings, it is more likely that the lake reloaded a number of times [*Kleinhans et al.*, 2005] during which the Gilbert-type delta built up more gradually and the Ma'adim Vallis experienced several stages of activity in agreement with the presence of terraces. Reloading and various stages of activity in outflow channels agrees with findings of *Ori and Mosangini* [1998]; *Ivanov and Head* [2001]; *Williams et al.* [2000]; *Williams and Malin* [2004]; and references therein. In short, these are indications that groundwater and lake reloading were common.

[88] A remarkable finding remains that all the calculated timescales are in the order of years to a few thousand years only, indicating very short periods for hydrological activity on the geological timescale of Mars. For Earth the small delta building timescales are known to be realistic because many deltas on Earth were created in the past thousands of years as a result of the post-glacial sea-level rise. This timescale hinges on the intermittency or continuity of the wet periods on early Mars, which is very uncertain for both the catastrophic mega-outflow channels and the smaller (sapping) valleys. Potentially the timescale of formation is very short but aquifer reloadings (of unknown duration) are necessary to explain the difference in sediment and water timescales.

8. Conclusions

[89] Flow discharge reconstruction and sediment transport estimates may constrain the duration of hydrological activity and the formation of channels and deltas on Mars. This, in turn, aids the understanding of the early Martian climate and ocean dynamics, which is still very limited. The aim of this paper was to contribute with a summary of up-to-date models for flow and sediment transport based on the fluvial geomorphology and civil engineering experience on Earth.

[90] The flow velocity and discharge can be calculated from channel depth and slope and the characteristics of the sediment on the channel floor. The Manning equation is unsuitable for this because it is dimensionally incorrect and a constant roughness is commonly assumed rather than a depth-dependent roughness as in the correctly nondimensionalized Darcy-Weisbach equations. To indicate the uncertainty of flow velocity, various roughness predictors are compared, including a new one derived from 190 rivers on Earth. The uncertainty for flow velocity is about a factor of 3, and for discharge a factor of 4 assuming some uncertainty in the water depth in otherwise well-constrained channel dimensions from MOLA or Mars Express HRSC altimetry.

[91] Next, the sediment mobility and the existence of bed forms can be predicted from the same flow characteristics. A nondimensionalized bed form prediction diagram also allows the estimation of possible flow conditions from bed form stratification or morphology.

[92] The grain size distribution of the sediment was inferred from lander information and from crater lake delta morphology. Unexpectedly, the evidence points toward bimodal sediment consisting of equal parts of coarse gravel/cobbles and silt/sand. The coarse part of the sediment is much coarser than previously assumed and strongly affects the hydraulic roughness and the sediment transport rates. However, unbiased samples are unavailable so the uncertainty of the sediment grain size distribution is large which also increases the uncertainty of hydraulic roughness and sediment transport.

[93] Commonly in previous work, the sediment transport is predicted from the assumption that 40% of the flow flux is sediment. This is only the case in special conditions, namely if the sediment consists of sand or silt, or if the sediment is supplied to the flow en masse and a hyperconcentrated flow emerges. This condition is at variance, however, with the existence of Gilbert-type crater lake deltas which are formed by bed load-dominated conditions and much smaller transport rates. Bed load will therefore have dominated in the smaller channels of Mars like those that were fed by sapping. The condition of hyperconcentration might, on the other hand, have dominated the initial stages of the largest outflow channels and contributed to the smooth deposits on the floor of the ancient ocean. A debris flow origin for the largest outflow channels is unlikely because the expected run-out lengths of the debris flows are much smaller than the lengths of the channels.

[94] Comparison of a number of sediment transport predictors for Martian conditions reveals, first, that the uncertainty of transport rate is an order of magnitude, and second, that the transport rates probably were much smaller than calculated when 40% of the flow volume is assumed to be sediment. A defendable choice of a sediment transport predictor is presented.

[95] Using the appropriate equations, the minimum timescales of hydrological activity and channel and delta formation were assessed for example cases. The results indicate very short formation periods for the channels and delta deposits, in agreement with deltas on Earth. The minimum timescale for hydrological activity is smaller than the minimum timescale for delta building, which indicates that many channels were formed in multiple events and several reloadings of the water sources must have occurred. The time period between reloading events, or the intermittency of a wet climate, is very uncertain and determines the true timescale.

[96] **Acknowledgments.** This paper would not have been written without the stimulating discussions with Stephan Van Gasselt and Ernst Hauber. I thank Ralf Jaumann for an opportunity to test an earlier version of this paper on the Planetology group at DLR, Francis Nimmo and Goro Komatsu for useful comments, Lionel Wilson for discussion on grain size distributions used in his 2004 paper and for a thorough and helpful review, Theo van Asch for discussion on debris flows, and Tanja Zegers and Bernard Foing of ESTEC for discussions on Ma'adim Vallis and Gusev Crater. The Netherlands Organisation for Scientific Research (NWO) and the Earth and Life Sciences council (NWO-ALW) are acknowledged for the personal "Veni" grant of the Innovational Research Incentives Scheme. Please contact M.G.K. for model runs at request.

References

Allen, J. R. L. (1984), *Sedimentary Structures, Their Character and Physical Basis*, 1256 pp., Elsevier, New York.

Allen, J. R. L., and M. R. Leeder (1980), Criteria for the instability of upper-stage plane beds, *Sedimentology*, *27*, 209–217.
Baas, J., W. van Kesteren, and G. Postma (2004), Deposits of depletive high-density turbidity currents: A flume analogue of bed geometry, structure and texture, *Sedimentology*, *51*, 1053–1088.
Bagnold, R. (1951), The movement of a cohesionless granular bed by fluid flow over it, *Br. J. Appl. Phys.*, *2*, suppl. 1, 29–34.
Bagnold, R. (1966), An approach to the sediment transport problem from general physics, U.S. Geol. Surv. Prof. Pap., *422-I*.
Baker, V. (2001), Water and the Martian landscape, *Nature*, *412*, 228–236.
Baker, V. (2002), High-energy megafloods: Planetary settings and sedimentary dynamics, *Spec. Publ. Int. Assoc. Sedimentol.*, *32*, 3–15.
Baker, V., and D. Milton (1974), Erosion by catastrophic floods on Mars and Earth, *Icarus*, *23*, 27–41.
Baker, V. R., R. G. Strom, V. C. Gulick, J. S. Kargel, and G. Komatsu (1991), Ancient oceans, ice sheets and the hydrological cycle on Mars, *Nature*, *352*, 589–594.
Berendsen, H., and E. Stouthamer (2000), Late Weichselian and Holocene palaeogeography of the Rhine-Meuse delta, The Netherlands, *Palaeo*, *161*, 311–335.
Burr, D. M., P. A. Carling, R. A. Beyer, and N. Lancaster (2004), Flood-formed dunes in Athabasca Valles, Mars: Morphology, modeling, and implications, *Icarus*, *171*, 68–83, doi:10.1016/j.icarus.2004.04.013.
Cabrol, N., and E. Grin (2001), The evolution of lacustrine environments on Mars: Is Mars only hydrologically dormant?, *Icarus*, *149*, 291–328, doi:10.1006/icar.2000.6530.
Cabrol, N., E. Grin, and G. Dawidowicz (1996), Ma'adim Vallis revisited through new topographic data: Evidence for an ancient intravalley lake, *Icarus*, *123*, 269–283.
Carr, M. (1996), *Water on Mars*, 229 pp., Oxford Univ. Press, New York.
Cenderelli, D., and E. Wohl (2003), Flow hydraulics and geomorphic effects of glacial-lake outburst floods in the Mount Everest region, Nepal, *Earth Surf. Processes Landforms*, *28*, 385–407.
Chadwick, A., and J. Morfett (1993), *Hydraulics in Civil and Environmental Engineering*, 2nd ed., 557 pp., E and FN Spon, New York.
Dietrich, W. (1982), Settling velocity of natural particles, *Water Resour. Res.*, *18*(6), 1615–1626.
Diplas, P., and J. Fripp (1992), Properties of various sediment sampling procedures, *J. Hydraul. Eng.*, *118*(7), 955–970.
Dunne, T. (1990), Hydrology, mechanics, and geomorphic implications of erosion by subsurface flow, in *Groundwater Morphology: The Role of Subsurface Water in Earth-Surface Processes and Landforms*, *Spec. Pap. Geol. Soc. Am.*, *252*, 1–28.
Einstein, H. (1950), The bed-load function for sediment transportation in open channel flows, *Tech. Bull. 1026*, Soil Conserv. Serv., U.S. Dep. of Agric., Washington, D. C.
Engelund, F., and E. Hansen (1967), *A Monograph on Sediment Transport in Alluvial Streams*, Teknisk Forlag, Kobenhavn, Denmark.
Fenton, L. K., J. L. Bandfield, and A. W. Ward (2003), Aeolian processes in Proctor Crater on Mars: Sedimentary history as analyzed from multiple data sets, *J. Geophys. Res.*, *108*(E12), 5129, doi:10.1029/2002JE002015.
Goldspiel, J., and S. Squyres (1991), Ancient aqueous sedimentation on Mars, *Icarus*, *89*, 392–410.
Golombek, M. P., A. F. C. Haldemann, N. K. Forsberg-Taylor, E. N. DiMaggio, R. D. Schroeder, B. M. Jakosky, M. T. Mellon, and J. R. Matijevic (2003), Rock size-frequency distributions on Mars and implications for Mars Exploration Rover landing safety and operations, *J. Geophys. Res.*, *108*(E12), 8086, doi:10.1029/2002JE002035.
Grotzinger, J., and Athena Science Team (2004), Stratification, sediment transport, and the early wet surface of Meridiani Planum, *Eos Trans. AGU*, *85*(47), Fall Meet. Suppl., Abstract P24A-01.
Hauber, E., et al. (2005), Delta-like deposits in Xanthe Terra as seen by the High Resolution Stereo Camera (HRSC), in *1st Mars Express Science Conference, 21–25 February 2005*, p. 28, ESA-ESTEC, Noordwijk, Netherlands.
Head, J., H. Hiezinger, M. Ivanov, M. Kreslavski, S. Pratt, and B. Thomson (1999), Possible ancient oceans on Mars: Evidence from Mars Orbiter Laser Altimeter data, *Science*, *286*, 2134–2137.
Head, J. W., L. Wilson, and K. L. Mitchell (2003), Generation of recent massive water floods at Cerberus Fossae, Mars by dike emplacement, cryospheric cracking, and confined aquifer groundwater release, *Geophys. Res. Lett.*, *30*(11), 1577, doi:10.1029/2003GL017135.
Herkenhoff, K., et al. (2004), Textures of the soils and rocks at Gusev Crater from Spirit's Microscopic Imager, *Science*, *305*, 824–826, doi:10.1126/science.1100015.
Hill, P., C. Lewis, S. Desmarais, V. Kauppaymuthoo, and H. Rais (2001), The Mackenzie Delta: Sedimentary processes and facies of a high-latitude, fine-grained delta, *Sedimentology*, *48*, 1047–1078.
Hoffman, N. (2000), White Mars: A new model for Mars' surface and atmosphere based on CO_2, *Icarus*, *146*, 326–342, doi:10.1006/icar.2000.6398.
Howard, A., R. Kochel, and H. Holt (1988), *Sapping Features of the Colorado Plateau*, *NASA Spec. Publ.*, *NASA SP-491*, 111 pp.
Hungr, O. (1995), A model for the runout analysis of rapid flow slides, debris flows, and avalanches, *Can. Geotech. J.*, *32*, 610–623.
Irwin, R., T. Maxwell, A. Howard, R. Craddock, and D. Leverington (2002), A large paleolake basin at the head of Ma'adim Vallis, Mars, *Science*, *296*, 2209–2212.
Irwin, R. P., III, A. D. Howard, and T. A. Maxwell (2004), Geomorphology of Ma'adim Vallis, Mars, and associated paleolake basins, *J. Geophys. Res.*, *109*, E12009, doi:10.1029/2004JE002287.
Ivanov, M., and J. Head (2001), Chryse Planitia, Mars: Topographic configuration, outflow channel continuity and sequence, and tests for hypothesized ancient bodies of water using Mars Orbiter Laser Altimeter (MOLA) data, *J. Geophys. Res.*, *106*(E2), 3275–3295.
Iverson, R. (1997), The physics of debris flows, *Rev. Geophys.*, *35*(3), 245–296.
Jerolmack, D. J., D. Mohrig, M. T. Zuber, and S. Byrne (2004), A minimum time for the formation of Holden Northeast fan, Mars, *Geophys. Res. Lett.*, *31*, L21701, doi:10.1029/2004GL021326.
Kleinhans, M. (2005a), Grain-size sorting in grainflows at the lee side of deltas, *Sedimentology*, *52*, 291–311, doi:10.1111/j.1365-3091.2005.00698.x.
Kleinhans, M. G. (2005b), Phase diagrams of bed states in steady, unsteady, oscillatory and mixed flows, in *Sandpit Project*, edited by L. C. V. Rijn et al., pp. Q1–Q16, Aqua, Amsterdam.
Kleinhans, M. G., and L. C. van Rijn (2002), Stochastic prediction of sediment transport in sand-gravel bed rivers, *J. Hydraul. Eng.*, *128*(4), 412–425.
Kleinhans, M., T. Zegers, B. Foing, R. Jaumann, G. Neukum, and HRSC Co-investigator Team (2005), Water and sediment dynamics and delta formation in Ma'adim Vallis and Gusev Crater, in *1st Mars Express Science Conference, 21–25 February 2005*, p. 152, ESA-ESTEC, Noordwijk, Netherlands.
Komar, P. (1979), Comparisons of the hydraulics of water flows in Martian outflow channels with flows of similar scale on Earth, *Icarus*, *37*, 156–181.
Komar, P. (1980), Modes of sediment transport in channelized water flows with ramifications to the erosion of the Martian outflow channels, *Icarus*, *42*, 317–329.
Kreslavsky, M. A., and J. W. Head (2002), Fate of outflow channel effluents in the northern lowlands of Mars: The Vastitas Borealis Formation as a sublimation residue from frozen ponded bodies of water, *J. Geophys. Res.*, *107*(E12), 5121, doi:10.1029/2001JE001831.
Krumbein, W., and F. Pettijohn (1938), *Manual of Sedimentary Petrography*, 549 pp., Appleton-Century-Crofts, New York.
Laity, J., and M. Malin (1985), Sapping processes and the developments of theater-headed valley networks on the Colorado Plateau, *Geol. Soc. Am. Bull.*, *96*, 203–217.
Leopold, L., M. Wolman, and J. Miller (1964), *Fluvial Processes in Geomorphology*, 522 pp., W. H. Freeman, New York.
Malin, M., and K. Edgett (2003), Evidence for persistent flow and aqueous sedimentation on early Mars, *Science*, *302*, 1931–1934, doi:10.1126/science.1090544.
Marion, A., and L. Fraccarollo (1998), A new conversion model for areal sampling of fluvial sediments, *J. Hydraul. Eng.*, *123*, 1148–1151.
Meyer-Peter, E., and R. Mueller (1948), Formulas for bed-load transport, in *Proceedings 2nd Meeting*, pp. 39–64, Int. Assoc. for Hydraul. Struct. Res., Stockholm.
Murray, J., et al. (2005), Evidence from the Mars Express High Resolution Stereo Camera for a frozen sea close to Mars' equator, *Nature*, *434*, 352–356, doi:10.1038/nature03379.
Nummedal, D., and D. Prior (1981), Generation of Martian chaos and channels by debris flows, *Icarus*, *45*, 77–86.
Ori, G., and C. Mosangini (1998), Complex depositional systems in Hydraotes Chaos, Mars: An example of sedimentary process interactions in the Martian hydrological cycle, *J. Geophys. Res.*, *103*(E10), 22,713–22,732.
Orton, G., and H. Reading (1993), Variability of deltaic processes in terms of sediment supply, with particular emphasis on grain size, *Sedimentology*, *40*, 475–512.
Parker, G. (1999), Progress in the modeling of alluvial fans, *J. Hydraul. Res.*, *37*(6), 805–825.
Parker, G. (2005), *Transport of gravel and sediment mixtures, in Sedimentation Engineering, ASCE Manual 54*, vol. 2, chap. 3, p. 131, Am. Soc. of Civ. Eng., New York. (Available at http://cee.uiuc.edu/people/parkerg/)
Parker, G., P. Klingeman, and D. McLean (1982), Bedload and size distribution in paved gravel-bed streams, *J. Hydraul. Eng.*, *108*(HY4), 544–571.

Parker, T. J., D. S. Gorsline, R. S. Saunders, D. C. Pieri, and D. M. Schneeberger (1993), Coastal geomorphology of the Martian northern plains, *J. Geophys. Res.*, *98*(17), 11,061–11,078.

Pirmez, C., and J. Imran (2003), Reconstruction of turbidity currents in Amazon channel, *Mar. Pet. Geol.*, *20*(6-8), 823–849.

Postma, G. (1995), Sea-level-related architectural trends in coarse-grained delta complexes, *Sediment. Geol.*, *98*, 3–13.

Powell, D. (1998), Patterns and processes of sediment sorting in gravel-bed rivers, *Progr. Phys. Geogr.*, *22*(1), 1–32.

Ribberink, J. S. (1998), Bed-load transport for steady flows and unsteady oscillatory flows, *Coastal Eng.*, *34*, 59–82.

Rickenmann, D. (1999), Empirical relationships for debris flows, *Nat. Hazards*, *19*, 47–77.

Russell, P. S., and J. W. Head (2003), Elysium-Utopia flows as mega-lahars: A model of dike intrusion, cryosphere cracking, and water-sediment release, *J. Geophys. Res.*, *108*(E6), 5064, doi:10.1029/2002JE001995.

Sharp, R., and M. Malin (1975), Channels on Mars, *Geol. Soc. Am. Bull.*, *86*, 593–609.

Silberman, E., R. Carter, H. Einstein, J. Hinds, R. Powell, and ASCE Task Force on Friction Factors in Open Channels (1963), Friction factors in open channels, *J. Hydraul. Eng.*, *89*(HY2), 97–143.

Simons, D., E. Richardson, and C. Nordin (1965), *Sedimentary Structures Generated by Flow in Alluvial Channels*, *Spec. Publ. Soc. Econ. Paleontol. Mineral.*, *12*, 34–52.

Sklar, L. S., and W. E. Dietrich (2004), A mechanistic model for river incision into bedrock by saltating bed load, *Water Resour. Res.*, *40*, W06301, doi:10.1029/2003WR002496.

Soulsby, R. (1997), *Dynamics of Marine Sands*, 215 pp., Thomas Telford, London.

Soulsby, R., and J. Damgaard (2005), Bedload sediment transport in coastal waters, *Coastal Eng.*, *52*(8), 673–689.

Southard, J. (1971), Representation of bed configurations in depth-velocity-size diagrams, *J. Sediment. Petrol.*, *41*(4), 903–915.

Southard, J. B., and A. L. Boguchwal (1990), Bed configurations in steady unidirectional water flows. Part 2. Synthesis of flume data, *J. Sediment. Petrol.*, *60*, 658–679.

Tanaka, K. (1999), Debris-flow origin for the Simud/Tiu deposit on Mars, *J. Geophys. Res.*, *104*(E4), 8637–8652.

Thatje, S., D. Gerdes, and E. Rachor (1999), A seafloor crater in the German Bight and its effect on the benthos, *Helgoland Mar. Res.*, *53*, 36–44.

Thiebodeaux, C., P. Washington, and R. De Hon (2003), Grain-size analysis of Maumee and Vedra channel sediments (Mars) using equilibrium sediment transport theory, in *Lunar Planet. Sci.*, *XXXIV*, p. 1268.

Van den Berg, J. (1995), Prediction of alluvial channel pattern of perennial rivers, *Geomorphology*, *12*, 259–279.

Van den Berg, J., and A. Van Gelder (1993), *A new bedform stability diagram, with emphasis on the transition of ripples to plane bed in flows over fine sand and silt*, *Spec. Publ. Int. Assoc. Sedimentol.*, *17*, 11–21.

Van Rijn, L. (1984a), Sediment transport, part I: Bed load transport, *J. Hydraul. Eng.*, *110*(10), 1431–1456.

Van Rijn, L. (1984b), Sediment transport, part II: Suspended load transport, *J. Hydraul. Eng.*, *110*(11), 1613–1641.

Walling, D., and D. Fang (2003), Recent trends in the suspended sediment loads of the world's rivers, *Global Planet. Change*, *39*, 111–126.

Williams, R. M. E., and M. C. Malin (2004), Evidence for late stage fluvial activity in Kasei Valles, Mars, *J. Geophys. Res.*, *109*, E06001, doi:10.1029/2003JE002178.

Williams, R., R. Phillips, and M. Malin (2000), Flow rates and duration within Kasei Vallis, Mars: Implications for the formation of a Martian ocean, *Geophys. Res. Lett.*, *27*(7), 1073–4076.

Wilson, L., and J. W. Head III (2004), Evidence for a massive phreatomagmatic eruption in the initial stages of formation of the Mangala Valles outflow channel, Mars, *Geophys. Res. Lett.*, *31*, L15701, doi:10.1029/2004GL020322.

Wilson, L., and P. J. Mouginis-Mark (2003), Phreatomagmatic explosive origin of Hrad Vallis, Mars, *J. Geophys. Res.*, *108*(E8), 5082, doi:10.1029/2002JE001927.

Wilson, L., G. J. Ghatan, J. W. Head III, and K. L. Mitchell (2004), Mars outflow channels: A reappraisal of the estimation of water flow velocities from water depths, regional slopes, and channel floor properties, *J. Geophys. Res.*, *109*, E09003, doi:10.1029/2004JE002281.

Wolman, M., and J. Miller (1960), Magnitude and frequency of forces in geomorphic processes, *J. Geol.*, *68*(1), 54–74.

Zanke, U. C. E. (2003), On the influence of turbulence on the initiation of sediment motion, *Int. J. Sediment Res.*, *18*(1), 1–15.

Zegers, T., et al. (2005), Geological mapping and structural analysis of Gusev area: A record of 4 GA of Martian history, in *1st Mars Express Science Conference, 21–25 February 2005*, p. 33, ESA-ESTEC, Noordwijk, Netherlands.

Zuber, M. T., D. E. Smith, S. C. Solomon, D. O. Muhleman, J. W. Head, J. B. Garvin, J. B. Abshire, and J. L. Bufton (1992), The Mars Observer Laser Altimeter investigation, *J. Geophys. Res.*, *97*(16), 7781–7797.

M. G. Kleinhans, Department of Physical Geography, Faculty of Geosciences, Utrecht University, P.O. Box 80115, 3508 TC Utrecht, Netherlands. (m.kleinhans@geo.uu.nl)

Correction to "Flow discharge and sediment transport models for estimating a minimum timescale of hydrological activity and channel and delta formation on Mars"

M. G. Kleinhans

Received 5 December 2005; published 10 January 2006.

Citation: Kleinhans, M. G. (2006), Correction to ''Flow discharge and sediment transport models for estimating a minimum timescale of hydrological activity and channel and delta formation on Mars,'' *J. Geophys. Res.*, *111*, E01002, doi:10.1029/2005JE002659.

[1] In "Flow discharge and sediment transport models for estimating a minimum timescale of hydrological activity and channel and delta formation on Mars" (*Journal of Geophysical Science*, *110*, E12003, doi:10.1029/2005JE002521, 2005), the work of *Irwin et al.* [2004] was not accurately represented in paragraph [87], for which I apologize. Paragraph [87] is corrected as follows:

[2] [87] Interestingly, also the large lake upstream of Ma'adim Vallis [*Irwin et al.*, 2002] must have reloaded (see Tables 2 and 3) if the mesas in the Gusev Crater are indeed the remains of a Gilbert-type delta as interpreted by *Cabrol et al.* [1996], *Irwin et al.* [2004], and *Zegers et al.* [2005]. If the sediment was mobile enough for hyperconcentration, then a Gilbert-type delta would probably not have formed. *Irwin et al.* [2004] therefore argued that the delta must have formed near the end of the flood. They calculated that the lake volume would be large enough to excavate Ma'adim Vallis in a single flood if the sediment concentration were 10% although they suggest that multiple lake overflows may have occurred. This concentration is two orders of magnitude larger than calculated in this paper. Given the present findings, it is more likely that the lake reloaded a number of times [*Kleinhans et al.*, 2005] during which the Gilbert-type delta built up more gradually and the Ma'adim Vallis experienced several stages of activity in agreement with the presence of terraces.

[3] In addition, two minor typing errors were made:

[4] In equation (8), the last constant should be 1.0864, not 6.24.

[5] In paragraph [75], the unit of the source area is km^2, not km^3.

0148-0227/06/2005JE002659$09.00

Additional corrections found over time...

Table 2. The Volume is in 10^6 km^3.